Palaeogeography, Palaeoclimatology, Palaeoecology 470 (2017) 11–29

Contents lists available at ScienceDirect

Palaeogeography, Palaeoclimatology, Palaeoecology

journal homepage: www.elsevier.com/locate/palaeo

# Aeolianite, calcrete/microbialite and karst in southwestern Australia as indicators of Middle to Late Quaternary palaeoclimates

Matej Lipar [a,*], John A. Webb [a], Matthew L. Cupper [b], Ningsheng Wang [c]

[a] Environmental Geoscience, Department of Ecology, Environment and Evolution, La Trobe University, Melbourne, Bundoora, Victoria, 3086, Australia
[b] School of Earth Sciences, The University of Melbourne, Melbourne, Victoria 3010, Australia
[c] School of Geography, Environment and Earth Sciences, Victoria University of Wellington, Wellington 6140, New Zealand

ARTICLE INFO

*Article history:*
Received 25 September 2016
Received in revised form 15 December 2016
Accepted 16 December 2016
Available online 10 January 2017

*Keywords:*
Tamala limestone
Pleistocene
Holocene
Calcarenite
Glacial period
Interglacial period

ABSTRACT

The mid-Late Pleistocene and Holocene aeolianites of the Tamala Limestone on the northern Swan Coastal Plain in southwestern Western Australia consist of six members that show cyclic deposition of coastal aeolianite, overlain by calcrete/microbialite, karstified surface and palaeosol. Field work, combined with mineralogical, chemical, stable isotope analysis and uranium-thorium (U/Th) and optically stimulated luminescence (OSL) dating, provides an insight into the repetitive glacial and interglacial climatic periods over the past 500 kyr. Deposition of the carbonate aeolianites occurred during interglacial episodes (marine isotope stage (MIS) 1, 5, 7, 9, 11, and possibly 13), due to migration of coastal dunes under the influence of strong southerly to southwesterly winds. Rainfall was insufficient to support vegetation cover on the dunes, and so was probably limited or seasonal. The transition from interglacial to glacial climates was characterised by higher effective rainfall, accompanied by aeolianite dissolution and karstification. During the colder climates and less effective rainfall of the glacial periods, there was no carbonate sand deposition; instead laminated microbialite and/or laminar calcrete formed, followed by palaeosol formation. The oxygen isotope composition of the microbialites indicates average temperatures during glacial periods ~4 °C −8 °C lower than today, and $\delta^{13}C$ values demonstrate a higher proportion of C4 plants and therefore a drier or more seasonal climate. Data from individual members of the Tamala Limestone show that the wettest interglacial period was MIS 5, when extensive karstification and pinnacle development occurred, and rainfall was probably higher than at any other time in the past 500 kyr. Of the glacial periods, MIS 10 was relatively wet or less seasonal, whereas MIS 8 and the Last Glacial Maximum (LGM) were relatively dry and windy. The low rainfall during the peak of the glacial periods was probably intensified by colder water offshore, due to weakening of the Leeuwin Current and its replacement by the cold, north-flowing West Australian Current.



## 1. Introduction

Aeolianites (i.e. aeolian calcarenites or dune limestones) are characteristic of Quaternary shorelines in many parts of the world, and have been widely used for investigations of Quaternary climates and sea levels (e.g. Milnes et al., 1987; Kindler and Hearty, 1996; Brooke, 2001; Williams and Walkden, 2002; Mylroie, 2008; Porat and Botha, 2008; Murray-Wallace et al., 2010; Bateman et al., 2011; Lomax et al., 2011; Brooke et al., 2014). They are primarily highstand deposits (Fumanal, 1995; Carew and Mylroie, 1997; Hearty and Kindler, 1997; Murray-Wallace et al., 1998, 2001; Hearty and O'Leary, 2008), but there is evidence of dune deposition during intermediate and even low sea levels (e.g. Kaye, 1959; Kendrick et al., 1991; Muhs et al., 1993; Hearty and Vacher, 1994; Frechen et al., 2001; Price et al., 2001; Brooke et al., 2014). Aeolianites contain a rich history of offshore carbonate production and coastal environmental change (e.g. Ward, 1973; Gardner, 1983; Hearty and O'Leary, 2008; Mylroie, 2008; James and Bone, 2015), but because their deposition is related to the interactions of sea level, climate, inshore morphology and tectonism, they are complex systems not totally controlled by climatic factors (Gardner, 1983).

However, the surface of aeolianites provides additional evidence of climatic change through calcrete/microbialite deposition and karstification. The stable isotope analysis (oxygen and carbon) of calcretes can be used to interpret of palaeoprecipitation and palaeotemperatures (Cerling and Quade, 1993; Zanchetta et al., 2000; Tabor et al., 2002; Alonso-Zarza, 2003; Dworkin et al., 2005; Tabor and Montanez, 2005; Sikes and Ashley, 2007; Achyuthan et al., 2012), and karstification is an indicator of relatively humid climates (e.g. Wright, 1988) because rainfall must be sufficient to cause extensive carbonate dissolution (Smith and Atkinson, 1976; Dreybrodt and Gabrovšek,

* Corresponding author.
*E-mail address:* matej.lipar@gmail.com (M. Lipar).

http://dx.doi.org/10.1016/j.palaeo.2016.12.019
0031-0182/

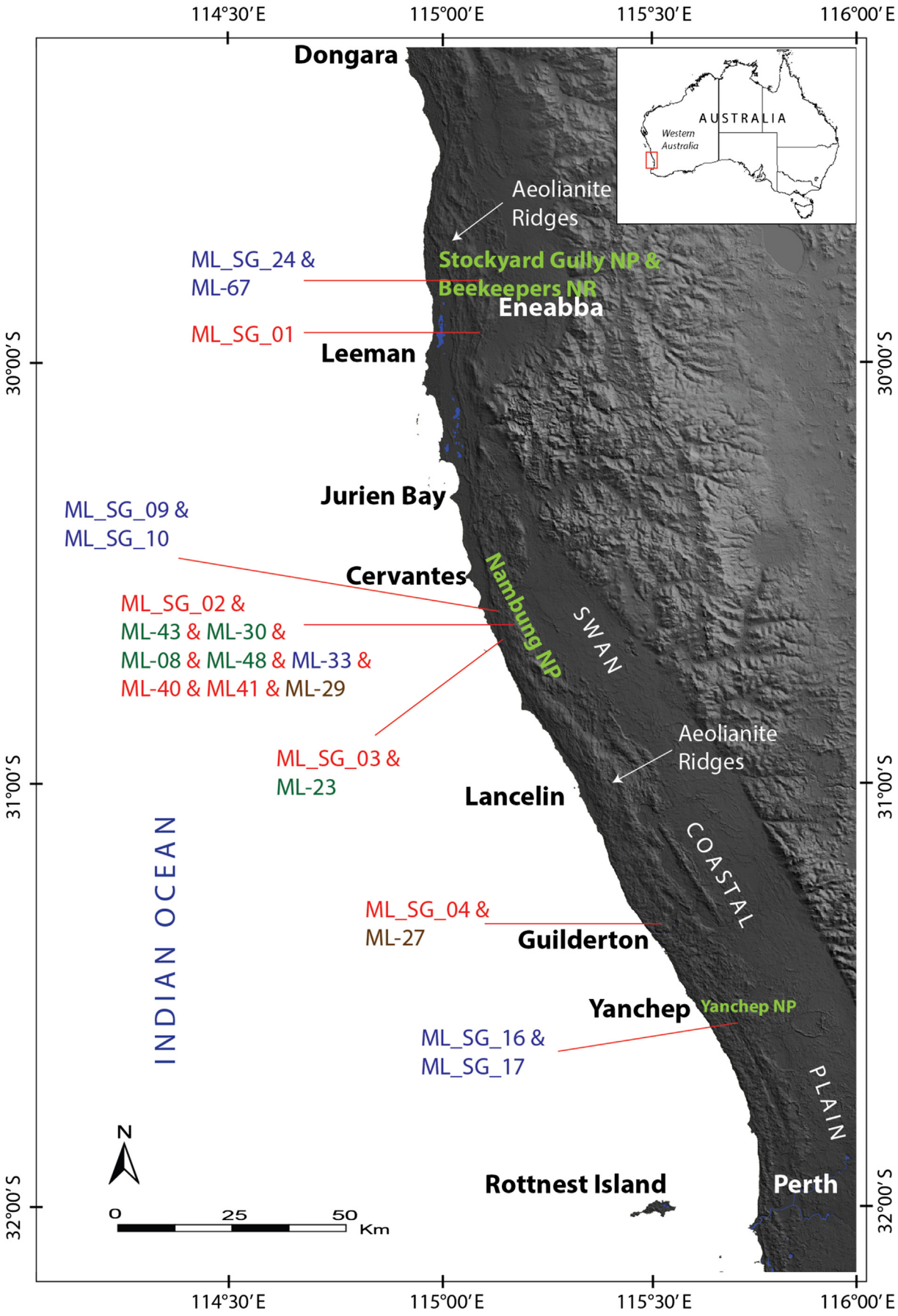
114°30′ E
115°00′ E
115°30′ E
116°00′ E
30°00′ S
31°00′ S
32°00′ S
Dongara
AUSTRALIA
Western Australia
Aeolianite Ridges
ML_SG_24 & ML-67
Stockyard Gully NP & Beekeepers NR
Eneabba
ML_SG_01
Leeman
Jurien Bay
ML_SG_09 & ML_SG_10
Cervantes
Nambung NP
SWAN
ML_SG_02 & ML-43 & ML-30 & ML-08 & ML-48 & ML-33 & ML-40 & ML41 & ML-29
ML_SG_03 & ML-23
Aeolianite Ridges
Lancelin
COASTAL
INDIAN OCEAN
ML_SG_04 & ML-27
Guilderton
Yanchep
Yanchep NP
ML_SG_16 & ML_SG_17
PLAIN
N
0 25 50 Km
Rottnest Island
Perth

2002; Ford and Williams, 2007). Temperature and carbon dioxide production are also important variables in karst development (White, 1988), but mean annual runoff is the principal determinant (Smith and Atkinson, 1976).

Furthermore, aeolianite karstification often results in the formation of caves containing secondary carbonate precipitates (speleothems; Frisia et al., 2000; Flügel, 2010), which can provide additional palaeoclimate information, as temperate humid climates are more favourable for speleothem formation than semi-arid to arid climates (Dreybrodt, 1980; Buhman and Dreybrodt, 1985; Genty and Quinif, 1996).

Therefore, the well-exposed aeolianites with extensive associated calcretes and karst on the northern Swan Coastal Plain in southwestern Western Australia provide an ideal opportunity to demonstrate how incorporating all these lines of evidence gives a more complete insight into Quaternary palaeoclimates than considering the aeolianites in isolation. This approach can potentially be applied to aeolianites worldwide, increasing the importance of this widespread coastal lithology in palaeoclimate interpretation.

## 2. Regional setting

The study area lies in southwestern Western Australia within the northern part of the Swan Coastal Plain, which extends west from a series of fault scarps to the Indian Ocean (Playford et al., 1976; Mory, 1995; Gozzard, 2007) (Fig. 1). This coastal plain is characterised by dune ridges on the coastal margin with an inner alluvial plain and colluvial slopes along the fault scarps (Jennings and Mabbutt, 1977; Pain et al., 2011).

The climate of southwestern Australia is Mediterranean with hot and dry summers, caused by a zone of high pressure (anticyclones) that passes over the region between October and March, and mild and wet winters, caused by subpolar, low-pressure cells that cross the region as cold fronts, usually accompanied by strong winds and cloudy skies (Davidson, 1995; Bureau of Meteorology, 2016). The coastal climate is also affected by the Leeuwin Current, a warm current which flows southwards along the Western Australian coast. This current increases the air temperature near the coast, resulting in convective rainfall inland (Cresswell, 1991; Reason et al., 1999; Luntz, 2004; Feng et al., 2009; Spooner et al., 2011); inshore meanders/eddies of the Leeuwin Current promote greater numbers of thunderstorms and heavy rainfall events onshore (Reason et al., 1999). Mean annual temperatures in southwestern Western Australia increase northwards from 18.3 °C in Perth to 20.7 °C in Eneabba with ~10 °C of seasonal variation (see Fig. 1 for locations). The average annual rainfall decreases from ~750 mm at Perth to ~490 mm at Eneabba with a winter maximum, and the average annual potential evaporation is ~1800 mm at Perth and increases northwards to ~2200 mm at Eneabba (Davidson, 1995; Bureau of Meteorology, 2016). The area is characterised by strong southerly winds; at Jurien Bay, in the windiest month (January), the winds blow from the south at >40 km/h for 50% of the time (3 pm wind speed) (Bureau of Meteorology, 2016).

The Swan Coastal Plain was originally covered by dense shrubby Kwongan heathland and Banksia or Tuart woodlands (Australia's Bioregions, 2012), but extensive areas have been cleared for farmland (Davidson, 1995). Generally, in the south the original vegetation was forest (Tuart and Jarrah) with a moderate to dense scrubby undergrowth (Playford et al., 1976), while in the north, low exposed heath with Acacia and Myrtles dominated the landscape, with Tuart woodlands in the valleys (Department of Conservation and Land Management, 1998). The change in vegetation reflects the northwards decrease in rainfall.

The Swan Coastal Plain is underlain by Permian to Early Cretaceous sediments of the Perth Basin. Derived by erosion of the Yilgarn Craton to the east, they extend offshore to the edge of the continental shelf (Playford et al., 1976; Jenkin, 1984; Cadman et al., 1994).

The surficial geology of the Swan Coastal Plain is characterised by young, mostly Quaternary sediments, mainly alluvial in the east and aeolian in the west (Mory, 1995; Gozzard, 2007). The aeolian sediments comprise three major dune systems, generally oriented parallel to the present coast and showing a progressive seawards decrease in age. From east to west these are the siliceous Bassendean Dune System (not discussed in this study), the carbonate Spearwood Dune System (Tamala Limestone), and the carbonate Quindalup Dune System (Safety Bay Sand) (Johnstone and Playford, 1955; Passmore, 1970; Playford and Low, 1971; Playford et al., 1976; Mory, 1995; Gozzard, 2007).

The Pleistocene Tamala Limestone is a morphostratigraphic unit of topographically irregular but generally subdued dune ridges (Playford et al., 1976, 2013; Mory, 1995; Playford, 1997; Gozzard, 2007). These barrier dunes stretch from Shark Bay in the north to the south coast of Western Australia (Playford, 1990), but related scattered outcrops appear as far north as Port Hedland and Broome (Teichert, 1947). The limestone consists predominantly of aeolian calcarenite, but there are also marine units, including shell beds (Teichert, 1947, 1950; Passmore, 1970; Playford et al., 1976; Kendrick et al., 1991; Gozzard, 2007). It is overlain by the Cooloongup Sand, which occurs as beds of loose yellow to red quartz sand up to several meters thick, and represents reworked insoluble residue of the Tamala Limestone (Lipar and Webb, 2014)

The Holocene coastal dune and marine deposits throughout the Swan Coastal Plain are grouped into the Safety Bay Sand (Passmore, 1970; Playford and Low, 1971). This consists of unconsolidated to weakly consolidated calcareous and quartzose sands (Passmore 1970; Playford and Low 1971; Playford et al. 1976; Semeniuk 1983, 1985; Gozzard 2007). Semeniuk (1983) defined three members of the Safety Bay Sand: in stratigraphic order, these are the weakly consolidated Burragenup Member and mobile Rosamel and Vittoria members. The Safety Bay Sand adjoins or covers the Tamala Limestone and Cooloongup Sand (Semeniuk 1983; Semeniuk et al. 1989; Mory 1995).

## 3. Methods

This study is based on detailed field mapping of the characteristics and extent of the Tamala Limestone and its topography between Perth and Dongara in southwestern Western Australia, focused on areas in the Nambung National Park, Beekeepers Nature Reserve and Stockyard Gully National Park (in the Eneabba region), near Guilderton, in Yanchep National Park, and in the Perth metropolitan area (Fig. 1).

Hand-sized, fresh rock samples as well as sand samples were examined in thin section for mineralogy and texture. The qualitative and quantitative mineral compositions were determined by X-ray powder diffraction (XRD) analysis, using the La Trobe University Siemens D5000 equipped with a Cu Kα source, operating at 40 kV and 30 mA in continual scan mode with a speed of 1°/min from 4° to 70° 2 Θ. Eva software was used for both qualitative and quantitative mineralogical analysis.

Speleothems, vein calcite and laminated microbialites lacking carbonate bioclasts were dated by the uranium-thorium (U/Th) method at the University of Melbourne and the University of Queensland (Table 1; see Figs. 1 and 2 for individual sample locations; dates previously published in Lipar and Webb, 2014). All ages were corrected for

**Fig. 1.** Locality map of northern Swan Coastal Plain in southwestern Western Australia. Location of dated samples: purple = U/Th flowstone, green = U/Th microbialite, red = OSL aeolianite, brown = OSL unconsolidated quartz sand. DEM downloaded from Shuttle Radar Topographic Mission website. (For interpretation of the references to colour in this figure legend, the reader is referred to the web version of this article.) (For interpretation of the references to colour in this figure legend, the reader is referred to the web version of this article.)

non-radiogenic $^{230}$Th incorporated at the time of deposition. Full details of the method are provided in Hellstrom (2003, 2006). Age errors are reported as 2σ uncertainties. Only one of the samples could not be dated precisely (ML_SG_24); it had a very low U/Th ratio so there is uncertainty in the assumptions for detrital corrections (Zhao et al., 2009). This sample was obtained from a stalagmite close to the collapse doline entrance of the cave, and was probably deposited under disequilibrium conditions due to evaporative effects.

Quartz sand samples from the Tamala Limestone and Cooloongup and Safety Bay Sands were dated by the optically stimulated luminescence (OSL) method at the University of Melbourne and at the Victoria University of Wellington, New Zealand (Table 2; see Figs. 1 and 2 for individual sample locations). The dates obtained by the University of Melbourne were published in Lipar and Webb (2014); additional dates were obtained for the present paper by Victoria University of Wellington for some previously undated members.

Calcarenite samples were collected by hammering off large blocks of indurated rock, and unconsolidated sand was sampled by driving 40 mm diameter PVC tubes into cleaned exposures. The light-exposed exteriors of the blocks and ends of the tubes were discarded and the samples were processed under subdued red light. The size fraction analysed (180–212 μm at University of Melbourne and 125–200 μm at Victoria University of Wellington) was extracted using standard procedures (e.g. Galbraith et al., 1999) and equivalent doses ($D_e$) estimated with a single-aliquot regenerative-dose (SAR) protocol (Murray and Roberts, 1998; Murray and Wintle, 2000).

For the OSL dating carried out at University of Melbourne, approximately 100 aliquots per sample, each composed of a single grain of quartz, were optically stimulated for 2 s at 125 °C by green (532 nm) light from a solid-state laser beam attached to an automated Risø TL-DA-15 apparatus (Markey et al., 1997; Bøtter-Jensen et al., 2000).

At Victoria University of Wellington Laboratory, 12–24 aliquots per sample (etched quartz grains 125–200 μm in diameter) were optically stimulated at 125 °C for 40 s by blue (470 nm) light using a Risø TL-DA-15 apparatus. In both laboratories, preheat and cut heat were 240 °C for 10 s, the Single Aliquot Regeneration Method (SAR) was applied (Murray and Wintle, 2000), and ultraviolet luminescence was detected using photomultiplier tubes with 7.5-mm Hoya U-340 filters.

Optical ages (reported as 2σ uncertainties) were derived from the weighted mean equivalent dose using the central age model of Galbraith et al. (1999). Fig. 3 shows the radial plots for all dated samples.

To determine the dose rate from the sample's burial environment (for the OSL dating carried out at University of Melbourne), the $^{40}$K, $^{238}$U and $^{232}$Th concentrations of the sample were measured using instrumental neutron activation analysis (INAA) by Becquerel Laboratories, Mississauga, Ontario, Canada. At Victoria University of Wellington Laboratory, the $^{40}$K, $^{238}$U and $^{232}$Th concentrations of the sample were based on the activity concentration of the nuclides $^{40}$K, $^{208}$TL, $^{212}$Pb, $^{228}$Ac, $^{214}$Bi, $^{214}$Pb and $^{226}$Ra measured by a high resolution and broad energy gamma spectrometer and analysed using GENIE 2000 software. Some samples display disequilibrium in their uranium decay chains, probably the result of radionuclide mobility during burial, but any adjustment for variation in the uranium content over time is negligible compared to the uncertainty of the calculated age.

Beta and gamma dose rates were calculated using the conversion factors of Guérin et al. (2011), with beta attenuation corrected using the factors devised by Mejdahl (1979) and attenuation of the beta and gamma rays by water using the sample moisture contents and corrections published in Aitken (1998). To determine the dose rate from cosmic rays, the depth of each sample below the surface was used along with its longitude, latitude and altitude, according to the formula of Prescott and Hutton (1994).

Some OSL samples could not be dated successfully. The luminescence curve for the Nambung Member was saturated, and the date from the Grey Member is too old, probably because the shallow depth (0.1 m) of this sample means the cosmic ray dose rate contribution was underestimated. Prescott and Hutton's (1994) equations for attenuation of muon intensity with depth are imperfect estimates for samples <0.6 m deep because they do not account for the soft components (electrons and photons) of cosmic rays, and this is particularly important for the Grey Member sample because the total dose rate is very low (Table 2).

Aeolianite and microbialite samples were analysed for both $\delta^{13}$C and $\delta^{18}$O isotopes at the stable isotope laboratory at the University of Melbourne. Four replicates of each sample were prepared for analysis in order to test the homogeneity of the samples following grinding, as well as to ensure that the instrument was producing reliable results. Analyses were performed on $CO_2$ produced by reaction of the sample with 100% $H_3PO_4$ at 90 °C using continuous-flow isotope ratio mass spectrometry (CF-IRMS), following the method previously described in Drysdale et al. (2009) and employing an AP2003 instrument. Results were reported using the standard δ notation (per mille ‰) relative to the Vienna Peedee Belemnite (VPDB) scale. Based on the following working standards, the uncertainty was 0.04‰ for $\delta^{13}$C and 0.07‰ −0.09‰ for $\delta^{18}$O (NEW 1: $\delta^{18}$O −2.46‰, $\delta^{13}$C +2.4‰; NBS-19: $\delta^{18}$O −2.2‰, $\delta^{13}$C +1.95‰; NBS-18: $\delta^{18}$O −23.05‰, $\delta^{13}$C −5.04‰; MOM: $\delta^{18}$O −4.84‰, $\delta^{13}$C −2.46‰).

## 4. Isotopic signatures of calcretes and their use for palaeoclimate interpretation

### 4.1. Oxygen isotopic signatures

The $\delta^{18}$O isotope composition of carbonates, including calcretes, is determined by the $\delta^{18}$O isotope composition of the water from which they precipitate and the temperature (Craig, 1965; Cerling, 1984; Hays and Grossman, 1991; Cerling and Quade, 1993). Consequently, the temperature at which calcrete formed can be calculated from the $\delta^{18}$O of the calcite and the water from which it precipitated:

$$1000\ \ln\alpha = 16.1\left(10^3 T^{-1}\right) - 24.6 \quad (1)$$

(Tremaine et al., 2011; based on speleothems)

$$1000\ \ln\alpha = 18.03\left(10^3 T^{-1}\right) - 32.17 \quad (2)$$

(Kim et al., 2007; based on synthetic carbonates)

$$\alpha = \frac{1000 + \delta(CaCO_3)}{1000 + \delta(H_2O)} \quad (3)$$

where $\delta(CaCO_3)$ is the $\delta^{18}$O of calcite relative to SMOW and $\delta(H_2O)$ is the $\delta^{18}$O of water relative to SMOW.

Calcretes precipitate from soil water that represents infiltrating rainfall (Cerling, 1984; Cerling and Quade, 1993; Jiamao et al., 1997; Zanchetta et al., 2000). In areas covered by vegetation, transpiration (non-fractionating) is the dominant mechanism for soil water loss, and evaporation (fractionating) is of little significance (Cerling, 1984), so the weighted average rainfall $\delta^{18}$O composition is very similar to that of soil water, and can be used for $\delta(H_2O)$ in Eq. (3).

This relationship holds in southwestern Western Australia, because the weighted average present $\delta^{18}$O rainfall composition (−4.06‰; calculated from the data in the Global Network of Isotopes in Precipitation and isotope Hydrology Information System (GNIP) for Perth) is very similar to the groundwater composition in the area (−4.06‰ to −4.09‰; Department of Water, 2012). This is typical of semi-arid climates (e.g. Turner and Thorpe, 2002; Liotta et al., 2013).

The oxygen isotopic values of groundwater in the Swan Coastal Plain dated to the last glacial period are ~0.5‰ lighter than present-day groundwater (Turner and Thorpe, 2002; Bekele et al., 2003);

**Table 1**
U/Th age data. All samples are composed of low-Mg calcite.

| Sample ID | Rock type | Location | Tamala Limestone member | 230Th/238U (A) | 95% ext. | 234U/238U (A) | 95% ext. | Age/Ka | 95%err | 232Th/238U (A) | 2se | 230Th/232Th (A) | Age 232Th corrected/Ka | 2se |
|---|---|---|---|---|---|---|---|---|---|---|---|---|---|---|
| ML-SG-24 | Stalagmite | Weelawadji Cave | ≥ Pinnacles Desert | 0.0255 | 0.0004 | 1.0497 | 0.0012 | 2.676 | 0.047 | 0.029240 | 0.000710 | 0.87 | 0.14 | 1.28 |
| ML-67 | Stalagmite | Weelawadji Cave | ≥ Pinnacles Desert | 0.0305 | 0.001 | 1.0370 | 0.0032 | 3.200 | 0.109 | 0.000687 | 0.000010 | 44.20 | 3.147 | 0.155 |
| ML-SG-17 | Stalagmite | Catacombs Cave | ≥ Pinnacles Desert | 0.0946 | 0.0006 | 1.0277 | 0.0010 | 10.529 | 0.075 | 0.023720 | 0.000230 | 3.99 | 8.43 | 1.06 |
| ML-SG-16 | Flowstone | Catacombs Cave | ≥ Pinnacles Desert | 0.1009 | 0.0007 | 1.0272 | 0.0011 | 11.268 | 0.080 | 0.010490 | 0.000100 | 9.62 | 10.35 | 0.47 |
| ML-SG-09 | Stalagmite | Brown Bone Cave | ≥ Pinnacles Desert | 0.1212 | 0.0006 | 1.0332 | 0.0009 | 13.596 | 0.077 | 0.021360 | 0.000170 | 5.67 | 11.72 | 0.94 |
| ML-SG-10 | Flowstone | Brown Bone Cave | ≥ Pinnacles Desert | 0.1727 | 0.0010 | 1.0790 | 0.0010 | 18.984 | 0.119 | 0.060970 | 0.000500 | 2.83 | 13.80 | 2.63 |
| ML-23[a] | Microbialite | Nambung NP | Grey | 0.5850 | 0.0026 | 1.0928 | 0.0034 | 82.198 | 0.599 | 0.055254 | 0.000499 | 10.59 | 74.01 | 8.82 |
| ML-43[a] | Microbialite | Nambung NP | Pinnacles Desert | 0.9819 | 0.0064 | 1.1468 | 0.0042 | 193.713 | 3.576 | 0.212765 | 0.002942 | 4.61 | 176.28 | 7.80 |
| ML-36[a] | Microbialite | Nambung NP | Pinnacles Desert | 0.9989 | 0.0041 | 1.0862 | 0.0033 | 250.083 | 4.627 | 0.242169 | 0.001659 | 4.12 | 207.15 | 56.63 |
| ML-08[a] | Microbialite | Nambung NP | Nambung | 1.0925 | 0.0036 | 1.1013 | 0.0023 | 354.114 | 9.173 | 0.100047 | 0.000531 | 10.92 | 341.61 | 17.98 |
| ML-48[a] | Microbialite | Nambung NP | Nambung | 1.1561 | 0.0120 | 1.1346 | 0.0028 | 406.485 | 37.708 | 0.345571 | 0.001051 | 3.35 | 382.70 | 44.54 |

[a] Dating results previously published in Lipar and Webb (2014, 2015).

temperatures at this time could have been ~5 °C colder (see later discussion), which indicates a variation of $\delta^{18}O$ of precipitation with surface air temperature (lapse rate) of ~0.1‰ $°C^{-1}$ for southwestern Western Australia. This is substantially less than the worldwide lapse rate of ~0.6‰ $°C^{-1}$ (Rozanski et al., 1992), and 0.3–0.39‰ $°C^{-1}$ in Mediterranean climates and China (Eriksson, 1965; Hauser et al., 1980; Jiamao et al., 1997).

Applying the difference in groundwater compositions between interglacial and glacial periods of approximately −0.5‰, the likely rainfall $\delta^{18}O$ composition in the study area during glacial periods would have been around 0.5‰ less than the present value of −4.06‰, i.e. −4.6‰. This value has been used to calculate palaeotemperatures for calcite precipitation in calcretes and microbialites during glacial periods (Table 3). The average present day rainfall composition (−4.06‰) was used to calculate palaeotemperatures for calcite precipitation during interglacial periods (Table 3).

The palaeotemperature calculations are based on assumptions which include considerable uncertainties. Nevertheless, the temperatures derived can be cross-checked against sample dates for consistency, e.g. the lower temperatures calculated from the isotopic composition of all the microbialites verify the dates indicating that the microbialites formed during glacial periods (as discussed in Section 6.3). The integration of the palaeotemperatures with the other data available (OSL and U/Th dates, carbon isotopes, stratigraphy, mineralogy, geomorphology) enhances the reliability of the climatic interpretations.

### 4.2. Carbon isotopic signatures

The $\delta^{13}C$ of soil carbonate (calcrete) depends on the isotopic composition of soil $CO_2$ (Quade et al., 1989) and fractionation between the different phases of the $CaCO_3$-$CO_2$-$H_2O$ system (Zanchetta et al., 2000). Soil $CO_2$ composition is controlled by the local vegetation (Cerling, 1984), in particular the ratio of C4 to C3 plants; C4 plants are warm season grasses, sedges and a few halophytic shrubs (Küçükuysal et al., 2012) and C3 plants are trees, most shrubs and herbs, and cool-season grasses (Jiamao et al., 1997; Azañón et al., 2006; Küçükuysal et al., 2012). The distribution and abundance of these plants are controlled by climate: C4 plants are adapted to higher water stress (lower and/or more unevenly distributed rainfall) and more elevated temperatures (Jiamao et al., 1997; Azañón et al., 2006; Küçükuysal et al., 2012). The relative abundance of C4 plants has been used as an index of past aridity (e.g. Jiamao et al., 1997).

C3 plants have $\delta^{13}C$ values between about −25‰ and −32‰, with a maximum frequency at about −27‰, while C4 plants have heavier values that vary between −10‰ and −14‰, with a maximum frequency at about −13‰ (Deines, 1980; Cerling and Quade, 1993). Consequently, the $\delta^{13}C$ of soil $CO_2$ is lighter when vegetation cover is dominated by C3 plants, and heavier when C4 plants predominate (Cerling, 1984; Alonso-Zarza, 2003). Soil $CO_2$ is not significantly influenced by atmospheric $CO_2$, because soil $P_{CO2}$ is much greater than $P_{CO2}$ in the atmosphere, and the amount of mixing is negligible below a depth of 30 cm (Zanchetta et al., 2000).

Diffusion coefficients for $^{12}CO_2$ and $^{13}CO_2$ in air differ by a factor of 1.0044, which causes the isotopic composition of soil $CO_2$ to be 4.4‰ enriched in $^{13}C$ relative to soil organic matter (Cerling, 1984; Wang and Zheng, 1989). Therefore, based on Cerling's (1984) model and Deines' (1980) data, $\delta^{13}C$ values for soil $CO_2$ produced by C4 plants (average $\delta^{13}C$ −13‰) would be about −8.6‰, and for that produced by C3 plants (average $\delta^{13}C$ −27‰) would be about −22.6‰. The fractionation of carbon between $CO_2$ and $CaCO_3$ is temperature dependent. Thus, at 13 °C, the likely mean annual temperature during glacial periods in the study area (see Section 6.3), the isotope fractionation factor is about −11.5‰ (Bottinga, 1969; Friedman and O'Neil, 1977), so the isotopic composition of soil carbonate precipitated at this temperature from $CO_2$ derived entirely from C4 plants is about +2.9‰, and for C3 plants about −11.1‰.

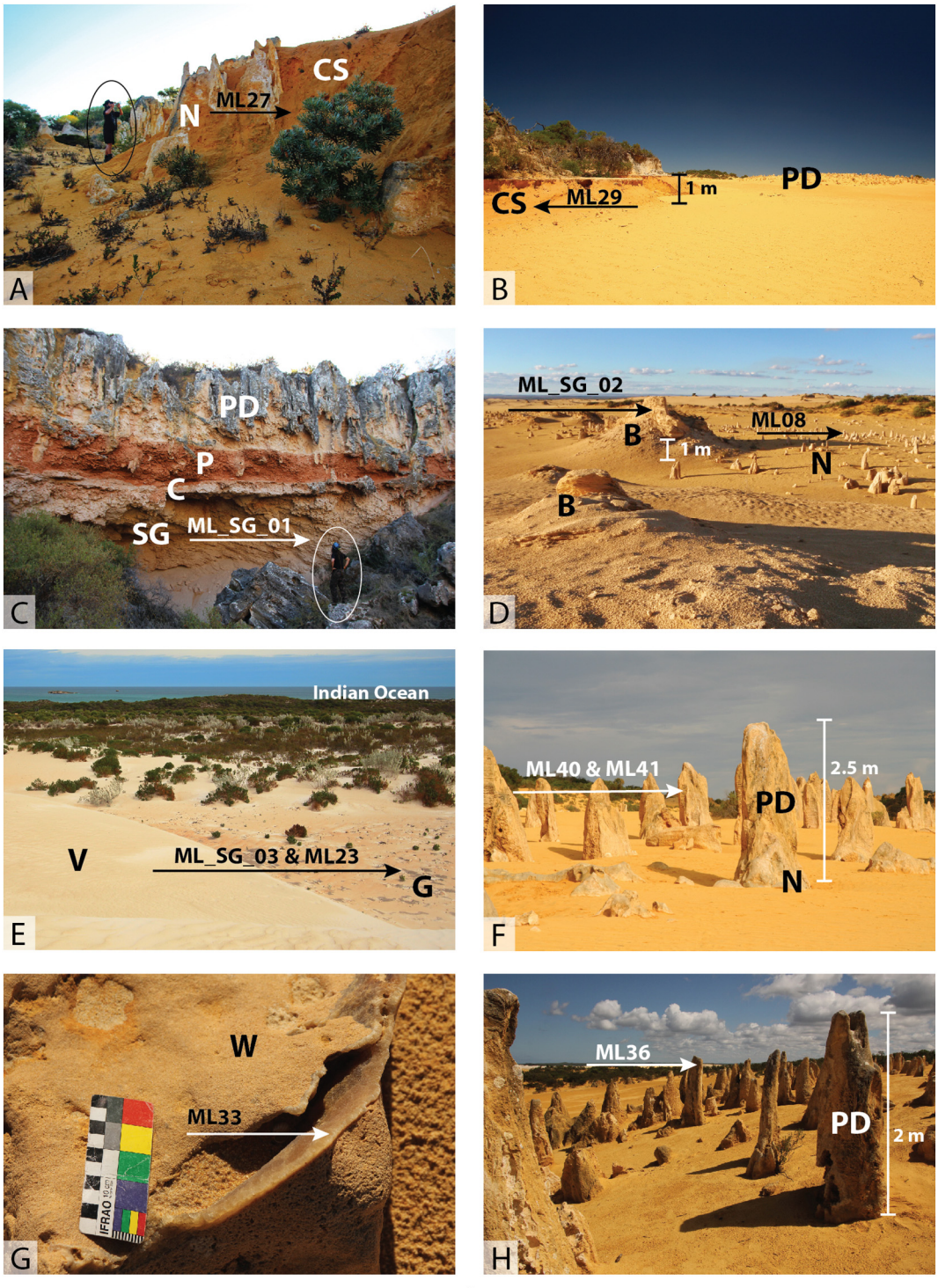


**Fig. 2.** A: Photographs of localities of dated samples (CS = Cooloongup Sand; N = Nambung Member; PD = Pinnacles Desert Member; SG = Stockyard Gully Member; W = White Desert Member; G = Grey Member; V = Vittoria Member; B = Burragenup Member; P = palaeosols; C = calcrete). (A) Exposure of the Cooloongup Sand and pinnacles near Guilderton; (B) an isolated mound of the Cooloongup Sand in the Pinnacles Desert, Nambung National Park; (C) a wall of the collapse doline in Beekeepers Nature Reserve with spectacular exposures of Tamala Limestone members; (D) Holocene aeolianite mounds and the pinnacles in The Pinnacles Desert, Nambung National Park; (E) exposure of the Grey Member and a recent unconsolidated calcareous sand dune in the southern part of Nambung National Park; (F) pinnacles in the Pinnacles Desert area, Nambung National Park; (G) calcite vein in the northern part of Nambung National Park; (H) pinnacles in the Pinnacles Desert area, Nambung National Park. See Fig. 1 for sample locations. B: Photographs of the localities of dates samples (N = Nambung Member; PD = Pinnacles Desert Member). (A) isolated pinnacles in the Pinnacles Desert area in Nambung National Park; (B) microbialite-pinnacle in the Pinnacle Desert area in Nambung National Park; (C) stalagmites at the entrance part of the Weelawadji Cave in Beekeepers Nature Reserve; (D) a column in the Brown Bone Cave in Nambung National Park with horizontal flowstone cemented on its surface; (E) flowstone and stalagmites in the Catacomb Cave in Yanchep National Park; (F) stalactites and stalagmites in the deeper section of the Weelawadji Cave in Beekeepers Nature Reserve. See Fig. 1 for sample locations. (For interpretation of the references to colour in this figure legend, the reader is referred to the web version of this article.) (For interpretation of the references to colour in this figure legend, the reader is referred to the web version of this article.)


B

**Fig. 2** (*continued*).

Wang and Zheng (1989) used this relationship to derive an equation for the carbonate isotopic composition in the soil; at 13 °C, this is:

$$\delta^{13}C_{CaCO3} = 2.9 \times C4 + (-11.1) \times (1-C4) \quad (4)$$

where C4 is the fraction C4 plants in the vegetation. It follows that the proportion of C4 plants in the local vegetation will be:

$$C4 = \left(11.1 + \delta^{13}C_{CaCO3}\right)/14.0 \,(\text{at } 13\ ^\circ\text{C}) \quad (5)$$

This equation can be modified for any temperature by substituting the fractionation factor for that temperature, and has been applied to the calcrete/microbialite of the different members of the Tamala Limestone, using the palaeotemperatures estimated from the $\delta^{18}O$ composition of the calcrete/microbialite (Table 3).

At present C4 grasses represent only 24% of grasses in the research area (Hattersley, 1983); assuming all the shrubs and trees are C3, this means that the present vegetation is dominated by C3 plants (probably ~90%). During the relatively dry glacial periods in this area (Wyrwoll, 1979, 1993; Tapsell et al., 2003), it might be expected that the proportion of C4 plants would have increased (Jiamao et al., 1997). However, at present C4 plants in Australia predominate in continental areas with strong seasonal rainfall and both C4 and C3 plants increase in number with increasing rainfall in their preferred temperature regime (Hattersley, 1983), meaning that their proportion in the research area can only be applied as a general indicator of aridity.

## 5. Results

### 5.1. Aeolian calcarenites

Six members have been recognised within the Tamala Limestone and Safety Bay Sand aeolianites on the northern Swan Coastal Plain; in stratigraphic order, these are the White Desert, Nambung, Stockyard Gully, Pinnacles Desert, Grey and Burragenup Members (Fig. 4; Lipar and Webb, 2014). Each member typically consists of aeolian calcarenite overlain by calcrete/microbialite and reddish-brown unconsolidated or weakly consolidated palaeosol; there may be a karst surface developed beneath the palaeosol, expressed as a weathered uneven surface with solutional voids filled with soil material.

The aeolianites are fine to coarse grained and well-sorted, containing variable amounts of carbonate (19–96%), quartz (4–79%), and feldspar (1–3%) (Lipar and Webb, 2014). They often show aeolian cross-bedding on weathered surfaces inclined up to 45° towards the north to north-east.

The carbonate component comprises detrital biogenic carbonate grains and carbonate cement. The bioclasts were originally composed either of aragonite (molluscs and some foraminifera) or high-Mg calcite (echinoderms, red-algae, foraminifera and some molluscs) (Lipar and Webb, 2014). These two minerals are stable only in the marine

**Table 2**
Luminescence age data.

| | Sample name | Rock type | Location | Depth (m) | Water[a] (%) | Radionuclide concentrations[b] | | | Environmental dose rate[c] (Gy ka-1) | Cosmic dose rate[d] (Gy ka-1) | Total dose rate[e] (Gy ka-1) | Equivalent dose[f] (Gy) | Optical age (ka; 2se) |
|---|---|---|---|---|---|---|---|---|---|---|---|---|---|
| | | | | | | K (%) | Th (ppm) | U (ppm) | | | | | |
| Victoria University of Wellington | ML_SG_02 | Calcarenite - Burragenup member | Nambung NP | 1.5 | 7.9 | 0.22 ± 0.01 | 0.70 ± 0.02 | 0.63 ± 0.05 | 0.39 ± 0.02 | 0.1627 ± 0.0081 | 0.55 ± 0.02 | 2.25 ± 0.17 | 4.1 ± 0.4 |
| | ML29[l] | Unconsolidated quartz sand - Cooloongup sand | Nambung NP | 1 | 6.7 | 0.84 ± 0.02 | 2.92 ± 0.04 | 0.39 ± 0.05 | 1.12 ± 0.03 | 0.1746 ± 0.0087 | 1.30 ± 0.04 | 40.30 ± 12.06 | 31 ± 7 |
| | ML27[l] | Unconsolidated quartz sand - Cooloongup sand | Near Guilderton | 1.5 | 6.9 | 1.68 ± 0.03 | 6.65 ± 0.09 | 1.03 ± 0.09 | 2.36 ± 0.06 | 0.1630 ± 0.0082 | 2.52 ± 0.06 | 124.64 ± 26.30 | >50 ± 11 |
| | ML_SG_03 | calcarenite - Grey member | Nambung NP | 0.1 | 9 | 0.10 ± 0.00 | 1.31 ± 0.03 | 0.91 ± 0.06 | 0.38 ± 0.02 | 0.1962 ± 0.0098 | 0.57 ± 0.02 | 150.76 ± 15.97 | 265 ± 29 |
| | ML_SG_01 | Calcarenite - Stockyard Gully member | Stockyard Gully NP | 4 | 7 | 0.34 ± 0.01 | 1.08 ± 0.03 | 0.43 ± 0.05 | 0.49 ± 0.02 | 0.1172 ± 0.0059 | 0.61 ± 0.02 | 189.51 ± 26.14 | 313 ± 44 |
| | Sample name | Rock type | Location | Depth (m) | Water[g] (%) | Radionuclide concentrations[h] | | | Environmental dose rate[i] (Gy ka-1) | Cosmic dose rate[j] (Gy ka-1) | Total dose rate (Gy ka-1) | Equivalent dose[k] (Gy) | Optical age (ka; 2se) |
| | | | | | | K (%) | Th (ppm) | U (ppm) | | | | | |
| University of Melbourne | ML41[l] | calcarenite - Pinnacles desert member | Nambung NP | 2 | 5 | 0.34 ± 0.02 | 3.7 ± 0.02 | 0.2 ± 0.01 | 0.63 ± 0.05 | 0.15 ± 0.02 | 0.77 ± 0.07 | 137 ± 19 | 177 ± 30 |
| | ML40[l] | calcarenite - Pinnacles desert member | Nambung NP | 2 | 5 | 0.41 ± 0.03 | 4.2 ± 0.03 | 0.6 ± 0.03 | 0.81 ± 0.07 | 0.15 ± 0.02 | 0.95 ± 0.10 | 173 ± 12 | 182 ± 23 |

[a] Measured as weight of water divided by dry weight of the sample taking into account a 25% uncertainty.
[b] Measured by gamma spectrometer in the laboratory. Gamma rays produced from sample material was counted for a minimum time of 24 h by a high resolution and broad energy gamma spectrometer. The spectra were then analysed using GENIE2000 software. The concentrations of U, Th and K were obtained by comparison with standard samples.
[c] Calculation was based on the activity concentrations of the nuclides $^{40}$K, $^{208}$Tl, $^{212}$Pb, $^{228}$Ac, $^{214}$Bi, $^{214}$Pb, $^{226}$Ra, using dose rate conversion factors published by Guérin et al. (2011).
[d] Determined by the depth of sample below the surface along with its longitude, latitude and altitude, convention formula and factors published by Prescott and Hutton (1994).
[e] Cosmic dose rate + environmental dose rate.
[f] Obtained by using SAR described by Murray and Wintle (2000), data was analysed by using Analyst programme.
[g] Estimated time-averaged moisture content, based on measured field water value (% dry weight).
[h] Obtained by INAA (Becquerel Laboratories, Mississauga, ON, Canada).
[i] Assumed internal alpha dose rate, plus beta dose derived from INAA radionuclide concentration measurements using the conversion factors of Guérin et al. (2011), corrected for attenuation by water and beta attenuation, plus gamma dose derived from INAA radionuclide concentration measurements using the conversion factors of Guérin et al. (2011), corrected for attenuation by water.
[j] Calculated using the equation of Prescott and Hutton (1994), based on sediment density, time-averaged depth and site latitude and altitude.
[k] Central age model (Galbraith et al. 1999), including a ± 2% systematic uncertainty associated with calibration of the laboratory beta-source.
[l] Dating results previously published in Lipar and Webb (2014, 2015).

environment, and under subaerial conditions they alter to low-Mg calcite (Bathurst, 1971; Reeckmann and Gill, 1981; Gardner, 1983). Therefore the aeolianite shows a progressive reduction with age in aragonite and high-Mg calcite content and a corresponding increase in low-Mg calcite content (Lipar and Webb, 2014), indicating that carbonate material from each depositional cycle was a fresh derivate from the ocean and not reworked from older aeolianites.

The grains in the aeolianites are cemented either by meniscus sparry calcite around grain contacts or drusy calcite that rims and sometimes fills pores. Microstalactitic (gravitational/pendant) cement, characterised by distinct thickening of cement crusts beneath grains, occurs occasionally, and echinoderm fragments are often surrounded by syntaxial rims. The presence of meniscus and pendant cement indicates that the lithification of the carbonate dunes occurred in a meteoric environment (vadose zone) (Scholle, 1978; Flügel, 2010).

The alteration of bioclasts and precipitation of cement due to meteoric processes is reflected in the whole rock carbon and oxygen isotopic values (Fig. 5), which become lighter with age due to more extensive diagenesis (e.g. Gardner, 1983; Beier, 1987). The relatively unaltered aragonite and high-Mg calcite marine skeletal grains of the uncemented Holocene sand have heavier values (~−0.3‰ $\delta^{18}$O, ~+0.9‰ $\delta^{13}$C) than the low-Mg calcite of the altered grains and meteoric cement of the older Tamala Limestone members (e.g. White Desert Member: ~−3.81‰ $\delta^{18}$O, ~−8.87‰ $\delta^{13}$C). This phenomenon has been described in Pleistocene limestones elsewhere in the world (Reeckmann and Gill, 1981; Gardner, 1983; Beier, 1987). The increasing meteoric diagenesis with age gives sufficiently distinctive whole rock $\delta^{18}$O compositions to differentiate the younger Burragenup, Grey and Pinnacles Desert Members (Fig. 5). The older members, in which the aragonite and high-Mg calcite have been entirely replaced by low-Mg calcite, have very similar stable isotope compositions.

### 5.2. Calcretes

Calcretes within the Tamala Limestone comprise whitish to yellowish (sometimes reddish) case-hardened indurated massive layers (up to ~50 cm thick; also termed hardpan calcrete), more strongly cemented than the calcarenite beneath due to additional micritic cement containing peloids and alveolar-septal structures. As a result the calcrete has a higher proportion of carbonate (~72% average; includes bioclasts and cement) than the unaltered calcarenite beneath (~57% average).

The presence of vadose meniscus and pendant cements within the aeolianites indicates that the overlying calcretes are of pedogenic origin

**Fig. 3.** Radial plots showing the dose distributions from the measured aliquots. The radial plots illustrate the distributions of ages for each aliquot (right-hand radial y-axis) relative to precision (x-axis). For sample locations and stratigraphy see Figs. 1 and 4.

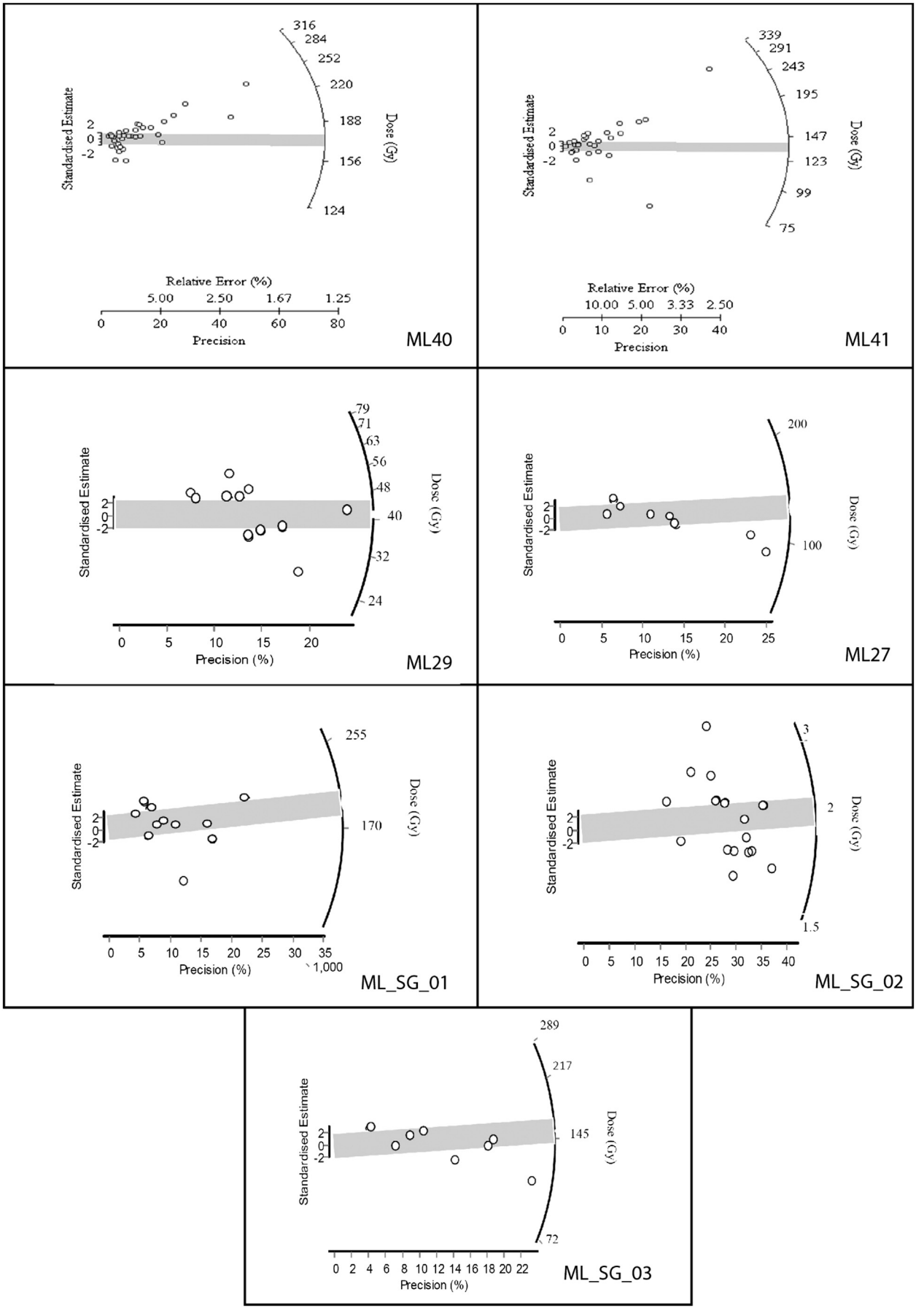
Standardised Estimate
Dose (Gy)
316
284
252
220
188
156
124
Relative Error (%)
5.00 2.50 1.67 1.25
Precision
ML40
339
291
243
195
147
123
99
75
10.00 5.00 3.33 2.50
ML41
79
71
63
56
48
40
32
24
Precision (%)
ML29
200
100
ML27
255
170
ML_SG_01
3
2
1.5
ML_SG_02
289
217
145
72
ML_SG_03

**Table 3**
Oxygen and carbon isotopic values of microbialites of Grey, Pinnacles Desert, Nambung and White Desert Members, and the vein within the White Desert Member; with calculated palaeotemperatures and proportion of C4 plants (see text for details).

| Stratigraphy | | | Isotopic composition (‰) | | Mean annual temperature (°C) | | Vegetation |
|---|---|---|---|---|---|---|---|
| Material | Sample | Age (MIS) | d18O (‰ PDB) | d13C (‰ PDB) | Kim et al. (2007) | Tremaine et al. (2011) | Proportion of C4 plants (%) |
| Grey M. (*microbialites*) | ML23[a] | 4 | −4.00 | −8.71 | 12 | 16 | 19.2 |
| | ML96 | 4 | −3.87 | −9.02 | 12 | 16 | 17.0 |
| | Median | 4 | −3.93 | −8.86 | 12 | 16 | 18.1 |
| Pinnacles Desert M. (*microbialites*) | ML36[a] | 6 | −3.63 | −8.37 | 11 | 15 | 19.5 |
| | ML42 | 6 | −3.69 | −8.78 | 11 | 15 | 16.6 |
| | ML43[a] | 6 | −3.61 | −8.27 | 11 | 14 | 20.2 |
| | ML44 | 6 | −3.61 | −8.74 | 11 | 14 | 16.9 |
| | ML62 | 6 | −3.86 | −8.78 | 12 | 16 | 16.6 |
| | ML75 | 6 | −3.63 | −9.12 | 11 | 15 | 14.1 |
| | ML81 | 6 | −3.62 | −8.80 | 11 | 14 | 16.4 |
| | Median | 6 | −3.63 | −8.78 | 11 | 15 | 16.6 |
| Nambung M. (*microbialites*) | ML01 | 10 | −4.01 | −9.97 | 12 | 16 | 10.2 |
| | ML06 | 10 | −3.97 | −9.33 | 12 | 16 | 14.8 |
| | ML08[a] | 10 | −3.78 | −8.92 | 11 | 15 | 17.7 |
| | ML26 | 10 | −3.90 | −9.33 | 12 | 16 | 14.8 |
| | ML39 | 10 | −3.90 | −9.22 | 12 | 16 | 15.6 |
| | ML48[a] | 10 | −3.73 | −9.43 | 11 | 15 | 14.1 |
| | ML52 | 10 | −3.92 | −9.04 | 12 | 16 | 16.9 |
| | ML53 | 10 | −3.88 | −8.94 | 12 | 16 | 17.6 |
| | ML54 | 10 | −3.92 | −9.52 | 12 | 16 | 13.4 |
| | ML60 | 10 | −3.78 | −9.15 | 11 | 15 | 16.1 |
| | ML61 | 10 | −3.83 | −9.28 | 12 | 16 | 15.2 |
| | ML89 | 10 | −3.82 | −9.03 | 11 | 15 | 16.9 |
| | Median | 10 | −3.89 | −9.25 | 12 | 16 | 15.4 |
| White Desert M. (*microbialites*) | ML45 | 12 | −3.47 | −8.09 | 10 | 14 | 20.8 |
| | ML46 | 12 | −3.70 | −8.53 | 11 | 15 | 17.6 |
| | ML47 | 12 | −3.38 | −8.77 | 10 | 13 | 15.9 |
| | Median | 12 | −3.47 | −8.53 | 10 | 14 | 17.6 |
| White Desert M. (*vein*) | ML33[a] | 13 | −4.54 | −9.64 | 17 | 22 | 16.1 |
| Present day | | | | | 19 | | est. < 10 |

[a] U/Th dated samples.

and did not form at water-table level (in which case the aeolianite cements would have phreatic textures).

Calcrete is present within most of the aeolianite members; the most abundant and thickest calcrete occurs in the Stockyard Gully Member with no evidence of a weathered (palaeo-karst) surface within or beneath it.

### 5.3. Microbialites

White to yellow laminated vadose (terrestrial) microbialites infill vertical karstic voids within the aeolianites. They have variable thickness (up to 2 m) and often column-like morphology (Fig. 6). The usage herein of the term 'microbialite' follows the definition of Wright (1989); "laminated, microbially formed structures which occur in vadose settings, either forming at the atmosphere-soil or sediment or rock interface, or within soil profiles".

The vadose origin of the microbialites in the Tamala Limestone is evident from the exclusively vadose cementation of surrounding aeolianite, which also contains pedogenic features like calcified roots. The microbialites grew within karst cavities in the aeolianites; similar terrestrial (vadose/subaerial) microbialites (stromatolites) have been documented in caves elsewhere (e.g., Cox et al., 1989; Lundberg and McFarlane, 2011). The microbialites have a different morphology to marine/lacustrine stromatolites (they are not columnar), and occur at all elevations in the Tamala Limestone rather than being restricted to a certain level (sea or lake level).

The predominantly vertical laminae of the microbialites are mostly composed of pure micrite, but some laminae contain floating quartz and feldspar grains (up to ~25%) (Fig. 6). The micritic laminae contain irregular alveolar-septal cavities, indicative of a microbial origin (Klappa, 1980; Adams and MacKenzie, 1998; Alonso-Zarza, 1999; Alonso-Zarza and Jones, 2007); these are often filled by calcite spar. Microbially induced irregular sub-spherical peloids are also present, formed of dense micrite with an alveolar-septal structure. The calcified microbial structures and wrinkled, contorted microfabric (Fig. 6) distinguish microbialites from abiogenic calcite precipitation, which is characterised by more even and finer lamination (Wright, 1989). Their organosedimentary origin is furthermore indicated by depleted stable carbon isotopes obtained from pure micrite layers (Fig. 7; Table 3); inorganic carbon would have a positive $\delta^{13}C$ value (Burne and Moore, 1987).

### 5.4. Palaeosols

Palaeosols occur on top of the calcarenite members and can be up to 1 m thick. They are a distinctive red or purple colour and contain a high percentage of silt-sized quartz along with some clay. They may contain abundant rhizoliths. Mineralogically, palaeosols comprise carbonate (bioclasts and cement; 25%–64%), quartz (33%–74%), and minor amounts of feldspar and clay (2–7%). The very fine grain size of the quartz and clay is indicative of an aeolian origin; these minerals were not derived by dissolution of the underlying aeolianite, which contains much coarser-grained quartz. The palaeosols are sometimes cemented by fine-grained sparry ferruginous calcite, occurring as menisci, pore-fills, and uniform concentric coatings around grains.

### 5.5. Karst

Numerous dissolution (karst) features are present in the Tamala Limestone, including well developed caves (Bastian, 1964, 2003; Jennings, 1968; Eberhard, 2004; Grimes, 2006) and surface depressions (collapse dolines and occasional solutional dolines; Jennings, 1968).

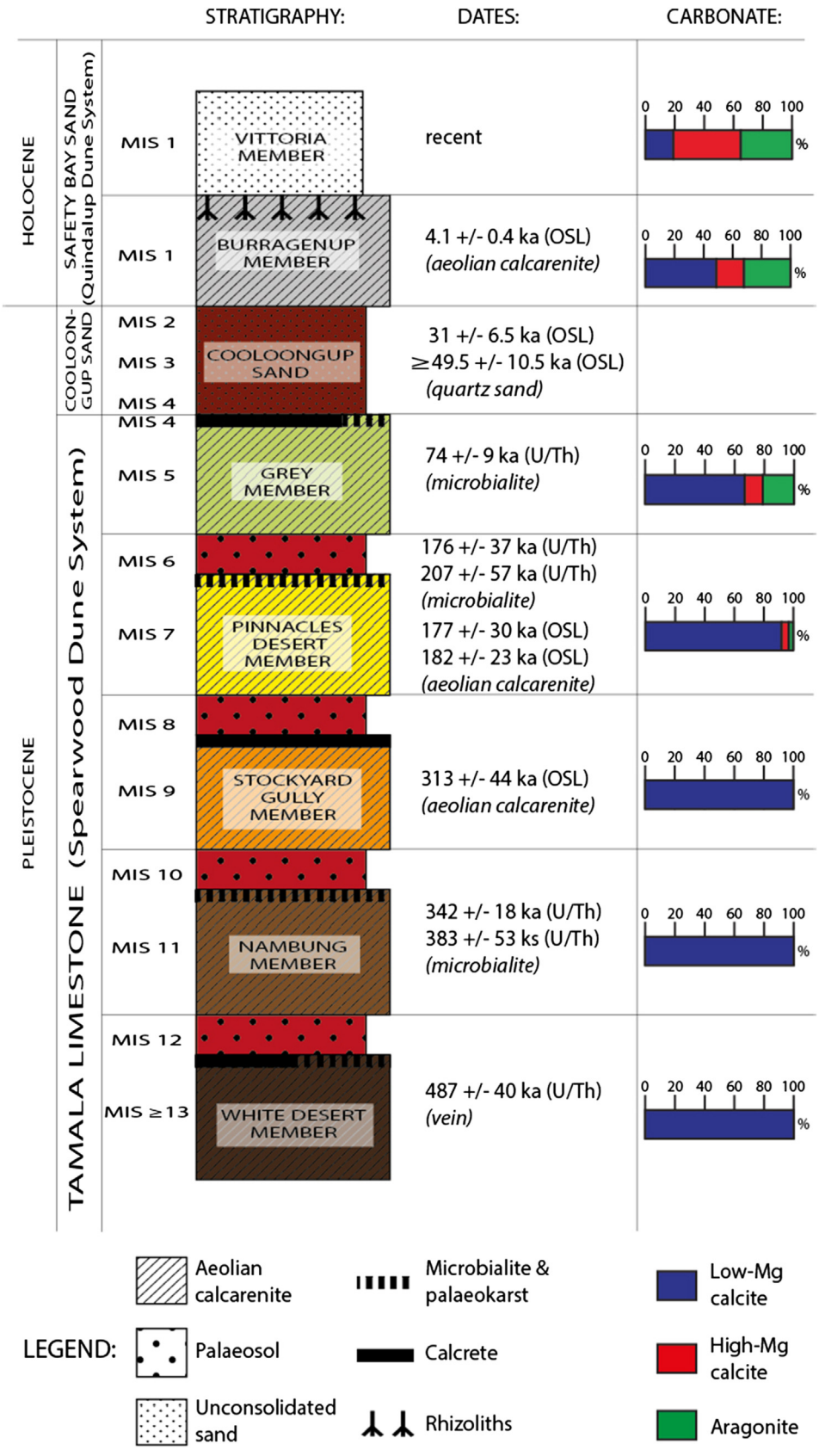


**Fig. 4.** Complete stratigraphy of the Tamala Limestone on the northern Swan Coastal Plain.

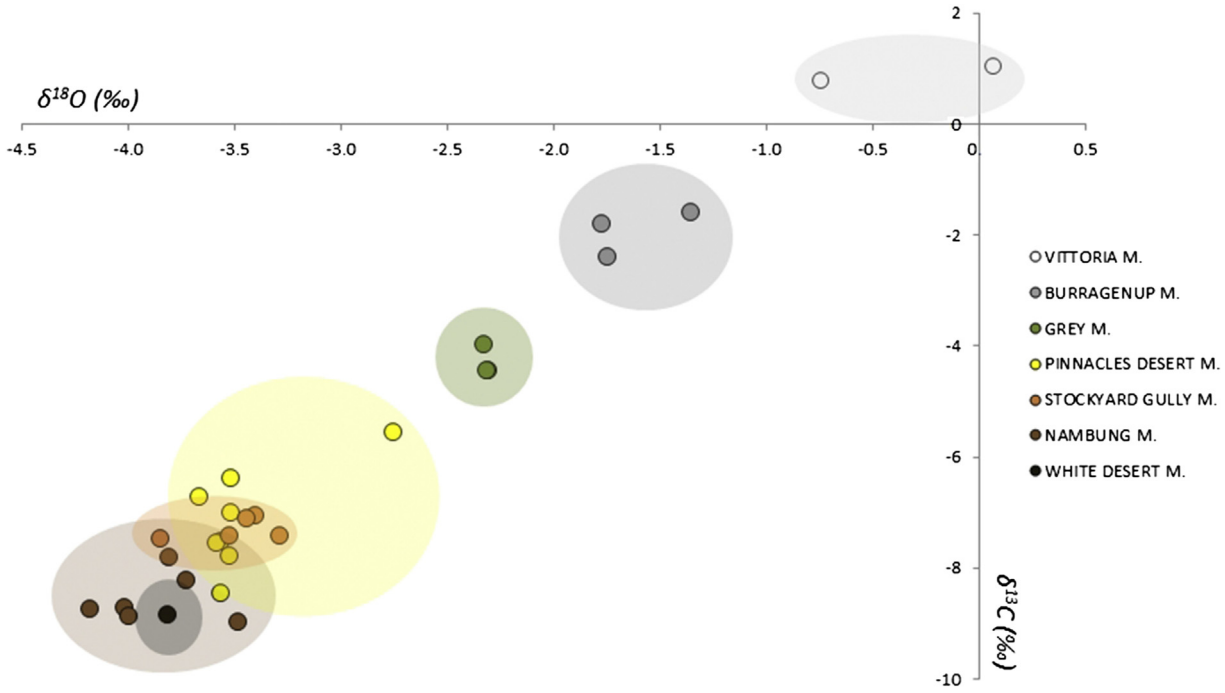


**Fig. 5.** Oxygen and carbon isotopic values of Tamala Limestone and Safety Bay Sand aeolianites and sands.

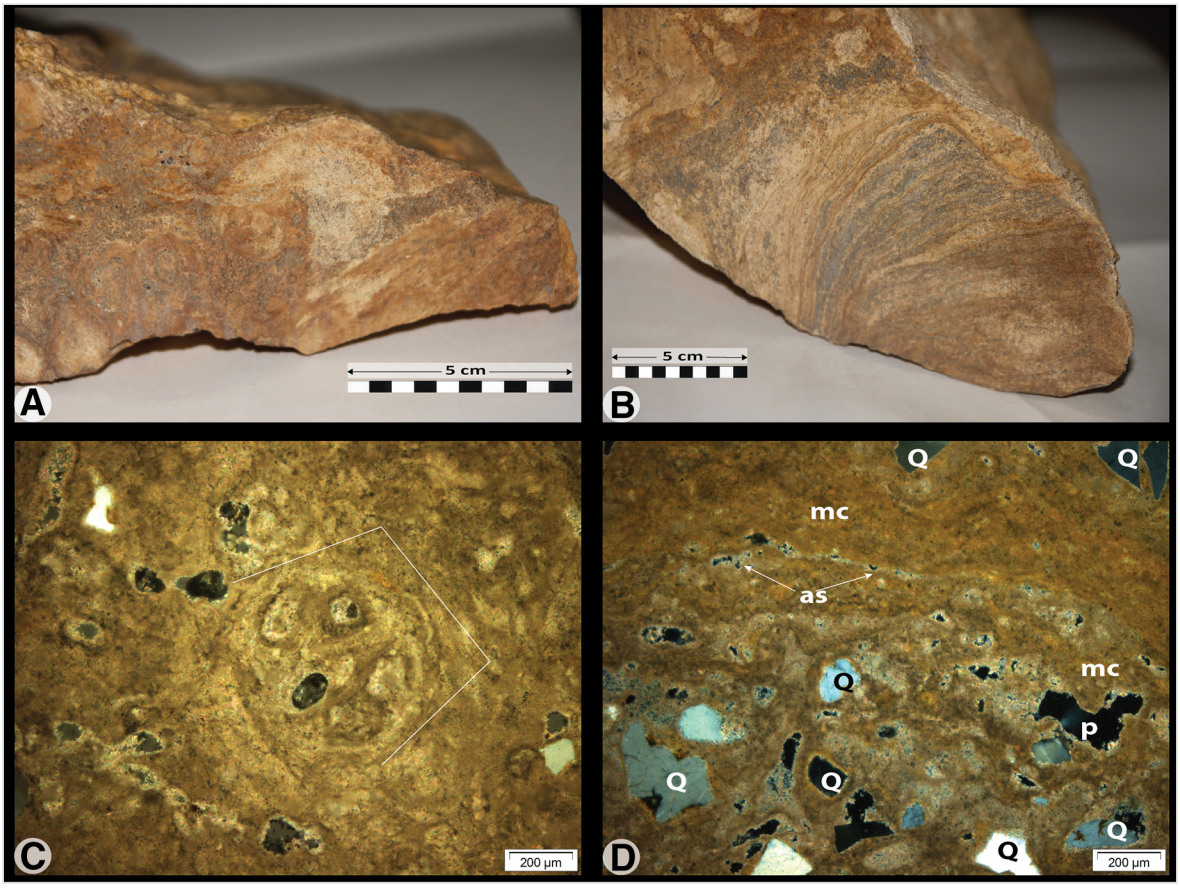


**Fig. 6.** Microbialite; A and B: a polished samples showing irregular laminae; C: thin section (in cross polarised light) showing irregular spherical peloid; D: thin section (in cross polarised light) showing floating quartz grains (Q), micritic cement (mc), porosity (p), and alveolar-septal structures (as).

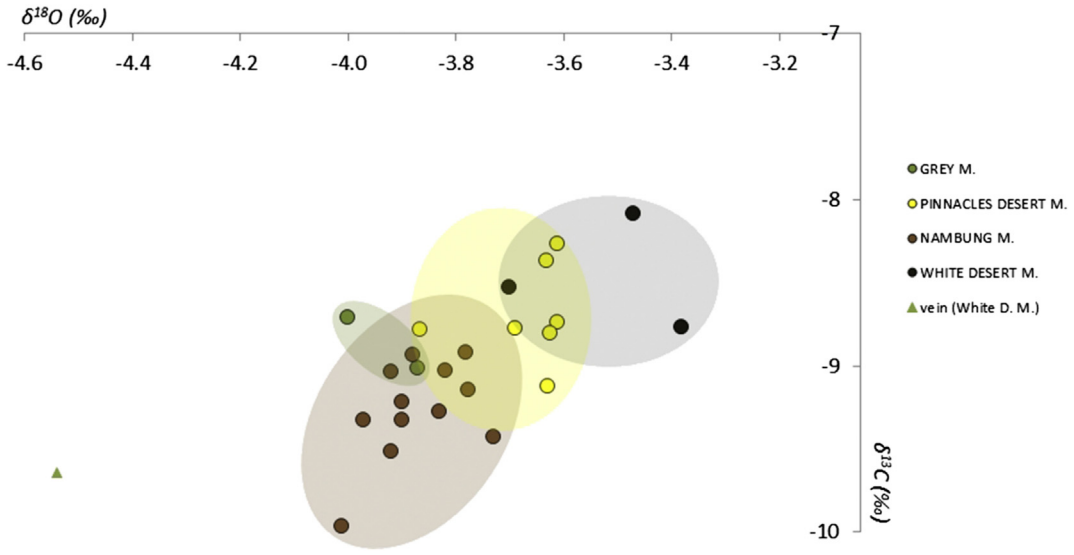


**Fig. 7.** Oxygen and carbon isotopic values of microbialites of Grey, Pinnacles Desert, Nambung and White Desert Members.

However, the most common surface karst features are solution pipes and pinnacles. Solution pipes are vertical tubular karst voids, commonly formed in porous carbonate rocks such as aeolianite during times of relatively high effective rainfall (Lipar et al., 2015). The expansion of solution pipes in the Tamala Limestone has left remnant limestone pinnacles (Lowry, 1973; Grimes, 2009; Lipar, 2009; McNamara, 2009; Hearty and Olson, 2011; Lipar and Webb, 2015), which are conical or cylindrical karst pillars. These provide excellent exposures of the stratigraphy of the Tamala Limestone, which can often be traced between adjacent pinnacles (Lipar and Webb, 2015). A karst surface with pinnacle development is present beneath the palaeosol at the top of several members of the Tamala Limestone, and although the pinnacles are often obscured by soil and sand cover, they are well exposed in limestone outcrops, along coastal cliffs and road cuttings, and can often be seen in cave walls and ceilings.

Speleothems (stalagmites, stalactites and flowstone) are common in caves of the northern Swan Coastal Plain, although they are more abundant in caves south of Perth, reflecting the rainfall increase southwards. Only a few speleothems in the study area are currently active, and most speleothem deposition occurred when the climate was wetter.

## 6. Palaeoclimate interpretation

Australia's Quaternary climate has oscillated between dry and wet episodes broadly linked to the worldwide glacial and interglacial periods respectively (Nanson et al., 1992, Turney et al., 2006; Rojas et al., 2009; Williams et al., 2009). The accompanying sea-level changes caused cyclic deposition of Pleistocene aeolianites across southern Australia (Gardner et al., 2006; Hearty and O'Leary, 2008; Murray-Wallace et al., 2010; Lomax et al., 2011; Playford et al., 2013; Brooke et al., 2014); similar deposits occur in a range of locations worldwide (Brooke, 2001), e.g. Bahamian Islands (Mylroie, 2008) and South Africa (Porat and Botha, 2008; Bateman et al., 2011).

The aeolianite/karstification/microbialite and/or calcrete/palaeosol cycles identified in the Pleistocene aeolianites of the Tamala Limestone of the northern Swan Coastal Plain allow the overall late Pleistocene climate history of this region to be interpreted in more detail than has previously been possible, and in particular allow the relative intensity of each glacial/interglacial cycle to be ascertained (Fig. 8).

### 6.1. Interglacial periods

The mid-late Pleistocene interglacial periods were characterised by aeolianite deposition on the northern Swan Coastal Plain, forming a coastal limestone ridge up to 10 km wide and rising >100 m above sea level. The aeolianites were deposited by consistently south to southwesterly winds, demonstrated by the aeolian cross-bedding in all members of the Tamala Limestone, and represent predominantly highstand deposition (Hearty and O'Leary 2008). Studies in southeastern Australia (Murray-Wallace et al. 2001, Murray-Wallace 2002), South Africa (Bateman et al. 2011) and the Bahamian Islands (Mylroie 2008) have shown that Quaternary aeolianite beach ridges formed during highstands; any lowstand deposition was reworked by the subsequent sea level rise. In southwestern Australia the linear aeolianites ridges are less obvious but still evident in some areas (Fig. 1), and their location at the landward edge of the Tamala Limestone confirms their deposition predominantly during highstands. Shell beds of equivalent age occur on the seaward side of the ridges in places (Passmore 1970, Kendrick et al. 1991), and there was limited aeolianite deposition on lower lying near-coastal areas at intermediate sea levels (Playford et al. 2013; Brooke et al. 2014), but most of this was removed by later rises in sea level.

The oldest member of the Tamala Limestone on the northern Swan Coastal Plain, the White Desert Member, is cross-cut by a ~1 cm thick calcite vein dated as 487 ± 40 ka (U/Th; Table 1), suggesting that the aeolianite deposition occurred during interglacial MIS 13, although it could have been earlier. No other aeolianites of this age are known in southwestern Western Australia; the dune at Kings Park in central Perth area, originally dated as ~422 ka (MIS 13 or MIS 15; Price et al., 2001; Hearty and O'Leary, 2008) was redated by Brooke et al. (2014; MIS 9).

The oxygen isotopic composition of the vein (−4.54‰) indicates that the average temperatures during this interglacial period were relatively similar to the present (ΔT = −2 °C to +3 °C; Table 3). The calculated proportion of C4 plants (16%) was higher than today (~10%) and only slightly lower than during most of the glacial periods in this area (up to 18%; Table 5), suggesting that the interglacial climate at this time was relatively dry and/or seasonal.

The aeolianite of the Nambung Member was deposited during interglacial MIS 11, based on U/Th ages of overlying microbialites that formed in the following glacial period (342 ± 18 ka and 383 ± 53 ka; Table 1). OSL dating of the aeolianite (Table 2) was unsuccessful, as the UV luminesce growth curve was saturated. However, aeolianite deposition during MIS 11 was recorded from the Guilderton area (amino-acid racemisation dating; Hearty and O'Leary, 2008) and probably also near Perth (OSL age of lower aeolianite unit at Peppermint Grove, 415 ka; Brooke et al., 2014).

The aeolianite of the Stockyard Gully Member yielded an OSL age of 312.7 ± 44 ka, placing its deposition in the interglacial MIS 9 (Table 2). An almost identical OSL age of 310 ka was obtained from a dune at Kings Park in central Perth (Brooke et al., 2014).

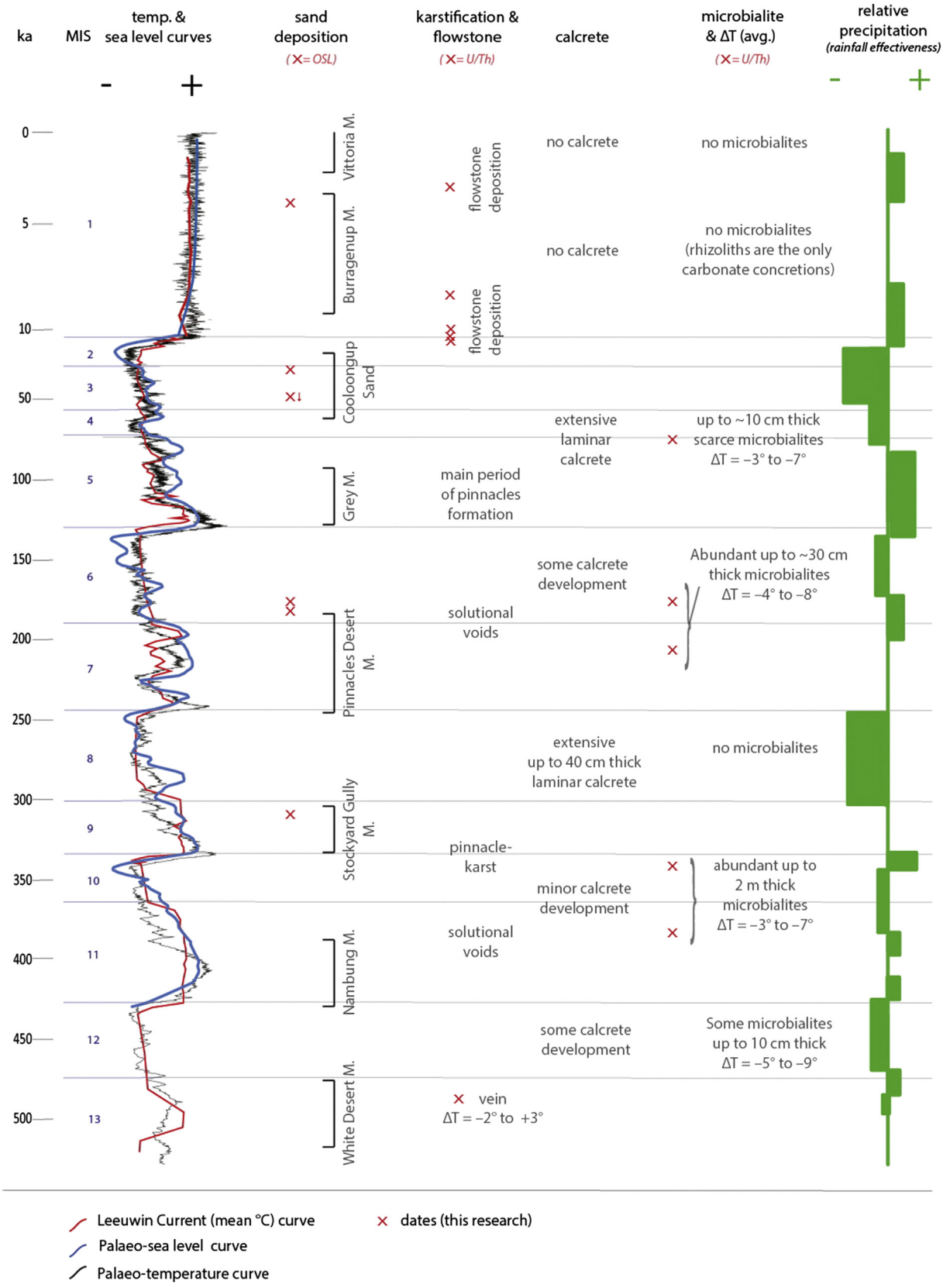


**Fig. 8.** The palaeoclimate history of the northern Swan Coastal Plain. Palaeotemperature curve from the European Project for Ice Coring in Antarctica (EPICA, Lemieux-Dudon et al., 2010; Jouzel et al., 2007), sea-level history from Waelbroeck et al. (2002), Leeuwin Current temperature history from Spooner et al. (2011).

Deposition of the aeolianite of the Pinnacles Desert Member probably occurred largely during MIS 7, based on U/Th dates from overlying microbialites of 207 ± 57 ka and 176 ± 37 ka (Table 1). Two aeolianite samples were OSL dated as 182 ± 23 ka and 177 ± 30 ka (Table 2), indicating that deposition extended into early MIS 6. Correlative OSL ages of of 205 ka and 230 ka (MIS 7) were obtained from the Tamala Limestone section at Zuytdorp Cliffs by Playford et al. (2013).

The Grey Member aeolianite is overlain by microbialite dated using the U/Th method as 74 ± 9 ka (late MIS 5 to early MIS 4; Table 1), so was most probably deposited in MIS 5. The calcreted (case-hardened) upper layer of this member yielded an OSL age of 264 ± 29 ka (Table 2), but this is believed to be too old as previously discussed.

Limited aeolianite deposition during MIS 5 occurred elsewhere in southwestern Western Australia (Hearty, 2003; Brooke et al., 2014) and in southeastern Australia (e.g. Gardner et al., 2006). The relative lack of aeolianite deposition at this time contrasts with the timing of aeolianite deposition of the other members of the Tamala Limestone, and probably reflects dune stability as a result of vegetation cover, due to the higher rainfall and perhaps weaker winds. MIS 5 was characterised by high effective rainfall in southwestern Australia, probably higher than at any other time in the last 500 kyr. This is shown by intense karstification during MIS 5 that formed the karst pinnacles of the Pinnacles Desert (Lipar and Webb, 2015) affecting microbialites of MIS 6 age (Pinnacles Desert Member); the pinnacles are overlain by the Cooloongup Sand, probably deposited in MIS 4-2 (discussed below). Evidence from the pollen record, coastal aeolianites and Murray Basin sediments in southeastern Australia also suggests that the last interglacial period was generally wetter than present (Harle, 1997; Murray-Wallace et al., 2000, 2010; Nanson et al., 2003; Gingele et al., 2004), and in eastern South Africa dune activity during MIS 5e was restricted by relatively warm and wet conditions (Porat and Botha, 2008).

The current interglacial period, characterised by the Holocene transgression (MIS 1), resulted in deposition of the Safety Bay Sand. The Burragenup Member yielded an OSL age of 4090 ± 340 yr BP (Table 2). Mory (1995) obtained a radiocarbon age of 8150 ± 270 yr BP (GS/CC Ref. 519) using biogenic carbonate grains from an outcrop on the northern Swan Coastal Plain, and Semeniuk (1985) estimated the age as 7700-5500 a based on radiocarbon ages from overlying, adjoining and underlying units on the Leschenault Peninsula, ~130 km south of Perth. The OSL age obtained during this study represents the actual depositional age of the dunes; the biogenic carbonate grains dated by Mory (1995) formed earlier. The Burragenup Member was deposited during a relatively dry and windy period during the Holocene in southwestern Western Australia, preceded and succeeded by wetter periods, dated using speleothems (see next section) at 12–8 ka and ~3 ka respectively.

Aeolianites in the study area of the northern Swan Coastal Plain were therefore deposited by sea-level highstands during interglacial episodes MIS 1, 5, 7, 9, 11 and possibly 13, due to carbonate dune migration during the "wetter" interglacial climates rather than the "drier" glacial periods. However, dune migration would not have been possible if the climate was consistently wet enough to support vegetation cover on the dunes, so precipitation was probably limited, less effective, or at least seasonal (as also shown by Stuut et al., 2014), and accompanied by strong predominantly southerly to southwesterly winds. The originally similar mineralogy and stable isotopic composition of carbonate grains within the aeolianites, along with the consistent cement textures, indicates that the aeolianites were all derived from the same material and deposited under the same environmental conditions.

### 6.2. Transition between interglacial and glacial periods

Following aeolianite deposition, the calcareous dunes became stabilised by vegetation and karstification occurred, forming a well-developed karst surface characterised by solutional voids and pinnacles (Lipar and Webb, 2015). This suggests that the transition between interglacial and glacial periods was characterised by relatively higher effective rainfall, probably due to decreasing temperatures but continued humid conditions, so evaporation was reduced. Lacustrine and speleothem studies in southeastern Australia (Kershaw and Nanson, 1993; Ayliffe et al., 1998; Desmarchelier et al., 2000) show higher lake levels and more speleothem formation during the transition from interglacial to glacial periods, confirming the higher effective precipitation at this time.

The decrease in height of the karst pinnacles northwards from Nambung National Park to the Eneabba region (Lipar and Webb, 2015) could therefore reflect a trend of northward-decreasing rainfall, as occurs in this part of southwestern Western Australia at present.

A well-developed (palaeo)karst surface is present on the Nambung Member aeolianite, exposed within cave and doline walls as columns up to 2 m wide and >2 m high, and formed during a period of extensive karstification probably in the transition from MIS 11 to MIS 10. In contrast, the practically complete lack of karstification on the Stockyard Gully aeolianite indicates a relatively dry phase during the transition from interglacial MIS 9 to glacial MIS 8.

The outcrops of the Pinnacles Desert Member were karstified during the transition from interglacial MIS 7 to glacial MIS 6, indicating a relatively wet episode (similar to that between MIS 11 and MIS 10) and were further karstified during the relatively wet MIS 5 climate, which was responsible for the main period of pinnacle development (see previous section). The following transition between interglacial MIS 5 and glacial MIS 4 was characterised by progressive drying towards a relatively dry and/or seasonally more variable climate, that favoured microbialite deposition in late MIS 5 and early MIS 4 (see below).

Higher effective rainfall during the most recent transition between glacial and interglacial periods (MIS 2) is indicated by substantial speleothem precipitation during 12–8 ka (Table 1) and the development of a karst surface dominated by solution pipes on younger aeolianites (late MIS 5 or younger) in low lying areas closest to the present-day coastline. Speleothem precipitation also occurred around 3 ka (Table 1), with a dry period from 3 to 8 ka (indicated by the Burragenup aeolianite deposition; see previous section). This evidence of Holocene climate variability is in accordance with other Holocene studies across southern Australia (e.g., Semeniuk, 1986; Gouramanis et al., 2012; Gliganic et al., 2014), including higher lake levels in the early Holocene followed by drier conditions in the mid Holocene (Kendrick, 1977; Rognon and Williams, 1977; Yassini and Kendrick, 1988; Harrison, 1993; Zheng et al., 2002).

### 6.3. Glacial periods

The microbialites in the Tamala Limestone were deposited in karst voids during glacial climates as demonstrated by their ages and oxygen isotope compositions, which indicate average temperatures ~4 °C–8 °C lower than today (Table 3), matching estimates of 5 °C to 10 °C lower temperatures during glacial periods elsewhere in Australia (Turney et al., 2006; Rojas et al., 2009). The laminar calcretes also formed in glacial climates; although they could not be dated due to the high content of calcite bioclasts, their stratigraphic position in the Tamala Limestone members is equivalent to the microbialites. The dominance of either microbialite or laminar calcrete deposition during each glacial period was probably due to differences in rainfall effectiveness. The palaeosol at the top of each member of the Tamala Limestone contains aeolian silt and clay deposited by the high winds associated with glacial climates. The formation of microbialites, calcrete and palaeosols followed karst dissolution of the limestone, suggesting that rainfall was relatively lower and/or less effective during the glacial periods in comparison to the transitional periods before and after. This matches evidence of significant aridity and stronger (or more effective) trade winds during glacial periods in Southwestern Australia (Parkin, 1974; Molina-Cruz, 1977; Wyrwoll, 1979, 1993; Tapsell et al., 2003) from aeolian and lacustrine sediments (Zheng et al., 2002), deep-sea sediments (Stuut et al., 2014) and pollen (Pickett et al., 2004).

The calcrete and minor microbialite on top of the White Desert Member aeolianite were probably deposited during the glacial period of MIS 12 (the microbialite could not be dated because of high contamination with detrital Th), during a drier or more seasonal climate (from the higher proportion of C4 plants; 17.6%; Table 3) that was about 5 °C to 9 °C colder than present (Table 3).

The laminated microbialites within the Nambung Member are the thickest of any member, and suggest about 3 °C–7 °C lower average temperatures and a climate with relatively low effective rainfall during the glacial period of MIS 10. The $\delta^{13}C$ values of the microbialites indicate a lower proportion of C4 plants in the vegetation compared to other glacial periods (Table 3), implying that MIS 10 was wetter or the seasonality of the rainfall was weaker, also shown by the almost complete absence of laminar calcrete.

Overlying the Stockyard Gully Member aeolianite is a 20- to 40-cm-thick massive hardpan calcrete (the thickest of all the Tamala Limestone members), followed by up to 1 m thick reddish palaeosol; no (palaeo)karst surface is evident. These indicate that the glacial climate of MIS 8 was drier and windier than in MIS 12 and 10 (and 6; see below).

The laminated microbialites of the Pinnacles Desert Member, deposited in glacial period MIS 6, indicate 4 °C–8 °C colder temperatures than present (based on the oxygen isotope values) and a relatively drier or seasonally more variable climate (based on the relatively high proportion of C4 plants) (Table 3).

The surface of the Grey Member is covered by up to ~10 cm thick microbialites and a laminar hardpan calcrete. The microbialites were deposited in the relatively drier or seasonally more variable climate of early MIS 4, as suggested by their age (74.0 ± 9 ka), 3 °C–7 °C lower average temperatures than present, and the relatively high proportion of C4 plants (Table 3). The laminar calcrete most probably formed in the following drier climate of late MIS 4.

The loose yellow to red quartzose Cooloongup Sand directly covers the Tamala Limestone, and was dated by OSL as 31 ± 6.5 ka and ≥49.5 ± 10.5 ka (≥MIS 3) (Table 2). The second OSL date is a minimum age as the growth curve indicates saturation. The grain size and composition of the Cooloongup Sand are virtually identical to the non-carbonate component of the Tamala Limestone, so the sand is most likely a residual material derived by dissolution of the limestone during the high rainfall in MIS 5 (Lipar and Webb, 2014). The extensive deposition of the Cooloongup Sand most probably spanned from MIS 4 to late MIS 2, and indicates a relatively dry and windy glacial climate, which is consistent with conditions during the Last Glacial Maximum elsewhere in Western Australia as well as in southeastern Australia (e.g. Harle, 1997; Shulmeister et al., 2004; Stuut et al., 2014). No calcrete or microbialites of this age have been found within the study area, probably because the on-going extensive deposition of quartz sand meant there was a lack of a stable substrate.

## 7. Influence of the Leeuwin Current on the pleistocene palaeoclimate in southwestern Western Australia

The Leeuwin Current transports warm low salinity water, formed within the Indonesian Warm Pool and the Central Indian Ocean, southwards along the southwestern Western Australian coastline, triggering convective rainfall inland. This current was continually present during the last ~550 kyr (Martinez et al., 1999; Barrows and Juggins, 2005; Spooner et al., 2011), but during glacial periods it was reduced in strength by shrinking of the Indo-Pacific Warm Pool, and the West Australian Current (a relatively cold northerly surface current off the Western Australian coast) was better developed (Barrows and Juggins, 2005).

The present study has shown that in southwestern Western Australia, there was an increase in effective rainfall in the transition from interglacial to glacial periods, causing karstification. This probably resulted from decreased evaporation due to reduction of average temperature, while at the same time the warm water of the Leeuwin Current was present offshore, so there was an overall increase in rainfall.

In the peak of the glacial periods, temperatures were lower (based on the stable isotope data from the microbialites), and if the subtropical high-pressure belt and the westerlies were displaced equatorward (northward) (e.g. Toggweiler et al., 2005; Sijp and England, 2008; Green and Pickering, 2014), this would have resulted in stronger winds in the study area, increasing the effect of evaporation and reducing the effective rainfall. This was probably reinforced by weakening of the Leeuwin Current and colder water offshore.

Fluctuations in the strength of the Leeuwin Current may also have been responsible for the different development of the microbialites in the Tamala Limestone. The very thick microbialites of the Nambung Member indicate a relatively humid glacial period during MIS 10, and this probably correlates with the prolonged presence of the Leeuwin Current off shore at this time (Spooner et al., 2011).

## 8. Conclusions

The mid-Late Pleistocene Tamala Limestone and Holocene Safety Bay Sand on the northern Swan Coastal Plain show cyclic deposition of coastal aeolianite, overlain by calcrete/microbialite, karstified surface and palaeosol. Dating and stable isotope analysis of the carbonates provides new insight into the repetitive glacial and interglacial climatic periods over the past 500 kyr.

Deposition of the aeolianites occurred during interglacial episodes (MIS 1, 5, 7, 9, 11, and possibly 13), in accordance with the predominantly highstand deposition of aeolianites elsewhere in Australia, and due to migration of coastal dunes under the influence of strong south to southwesterly winds. Rainfall was insufficient to support vegetation cover on the dunes, and so was probably limited or seasonal. Aeolianite deposition in the northern Swan Coastal Plain during MIS 5 occurred only at lower elevations and was probably restricted to 5c, reflecting high precipitation during the peak interglacial period (MIS 5e), so the dunes were vegetated and stabilised at that time.

The transition from interglacial to glacial climates was characterised by higher effective rainfall; the calcareous dunes were covered by vegetation and limestone dissolution and karstification occurred. This was probably due to decreased evaporation caused by the reduction in average temperature, reinforced by the on-going offshore presence of the warm water of the south-flowing Leeuwin Current, resulting in an overall increase in rainfall effectiveness. Virtually no karstification occurred during the MIS 9–8 transition, indicating a relatively dry phase, and contrasting with the intense karstification during MIS 5 that resulted in extensive pinnacle formation, due to the very wet climate (probably wetter than at any other time in the last 500 kyr).

During glacial periods the shift to colder climates with less effective rainfall and the absence of dune deposition caused laminated microbialite deposition in karst voids and/or laminar calcrete formation, followed by palaeosol formation. Palaeotemperatures ($\delta^{18}O$) from the microbialites indicate that average temperatures were ~4–8 °C lower than today during glacial episodes, and $\delta^{13}C$ values demonstrating a higher proportion of C4 plants suggest a drier or more seasonal climate. The thickest microbialites formed during MIS 10, when there was a lower proportion of C4 plants in the vegetation than in other glacial periods, implying that MIS 10 was wetter or less seasonal than other glacial periods. In contrast, a massive hardpan calcrete and relatively thick palaeosol were deposited during MIS 8, showing that the glacial climate at this time was relatively dry. The most recent glacial period (MIS 4-2) was similarly dry and also windy, causing laminar calcrete formation in MIS 4, and extensive deposition of quartzose sand in MIS 4-2. This sand is composed of residual material derived by dissolution of the limestone during the preceding high rainfall of MIS 5.

## Acknowledgments

We wish to thank Ken Grimes, Susan White, Andrej Kranjc, Colin Murray-Wallace and anonymous reviewers for comments on the early

draft of the text, and John Hellstrom and Jian-Xin Zhao for performing the U/Th analyses. We also wish to thank Western Australian Speleological Group (Inc.) for the agreement to use their reference sources and for organising and leading cave trips required for this research. A permit to conduct research in national parks as well as to enter certain caves or cave passages was obtained from the Western Australia Department of Environment and Conservation (now Department of Parks and Wildlife).

The research was carried out while the senior author was supported by a La Trobe University Postgraduate Research Scholarship and Australian Speleological Federation Karst Conservation Fund.

## References

Achyuthan, H., Shankar, N., Braida, M., Ahmad, S.M., 2012. Geochemistry of calcretes (calcic palaeosols and hardpan), Coimbatore, Southern India: formation and paleoenvironment. Quat. Int. 265, 155–169.

Adams, A.E., MacKenzie, W.S., 1998. A Colour Atlas of Carbonate Sediments and Rocks Under the Microscope. W.S. Manson Publishing (180 pp).

Aitken, M.J., 1998. An Introduction to Optical Dating: The Dating of Quaternary Sediments by the Use of Photon-stimulated Luminescence. Oxford University Press, Oxford.

Alonso-Zarza, A.M., 1999. Initial stages of laminar calcrete formation by roots: examples from the Neogene of central Spain. Sediment. Geol. 126, 177–191.

Alonso-Zarza, A.M., 2003. Palaeoenvironmental significance of palustrine carbonates and calcretes in the geological record. Earth-Sci. Rev. 60, 261–298.

Alonso-Zarza, A.M., Jones, B., 2007. Root calcrete formation on Quaternary karstic surfaces of Grand Cayman. Geol. Acta 5 (1), 77–88.

Australia's Bioregions IBRA, 2012: URL: http://www.environment.gov.au/parks/nrs/science/bioregion-framework/ibra/index.html#ibra (October, 2012).

Ayliffe, L.K., Marianelli, P.C., Moriarty, K.C., Wells, R.T., McCulloch, M.T., Mortimer, G.E., 1998. 500 ka precipitation record from southeastern Australia: evidence for interglacial relative aridity. Geology 26 (2), 147–150.

Azañón, J.M., Tuccimei, P., Azor, A., Sánchez-Almazo, I.M., Alonso-Zarza, A.M., Soligo, M., Pérez-Peña, J.V., 2006. Calcrete features and age estimates from U/Th dating: implications for the analysis of Quaternary erosion rates in the northern limb of the Sierra Nevada range (Betic Cordillera, southeast Spain). In: Alonnso-Zarza, A.M., Tanner, L.H. (Eds.), Paleoenvironmental Record and Applications of Calcretes and Palustrine Carbonates 416. Geological Society of America, pp. 223–239 (Special Paper).

Barrows, T.T., Juggins, S., 2005. Sea-surface temperatures around the Australian margin and Indian Ocean during the Last Glacial Maximum. Quat. Sci. Rev. 24, 1017–1047.

Bastian, L., 1964. Morphology and development of caves in the southwest of Western Australia. Helictite 2 (4), 105–119.

Bastian, L., 2003. Hydrogeology and speleogenesis update, the Yanchep Cave Area, Western Australia. 24th Biennial Conference of the ASF, pp. 36–44.

Bateman, M.D., Carr, A.S., Dunajko, A.C., Holmes, P.J., Roberts, D.L., Mclaren, S., Bryant, R.G., Marker, M.E., Murray-Wallace, C.V., 2011. The evolution of coastal barrier systems: a case study of the Middle–Late Pleistocene Wilderness barriers, South Africa. Quat. Sci. Rev. 30, 63–81.

Bathurst, R.G.C., 1971. Carbonate sediments and their diagenesis. Developments in Sedimentology 12. Elsevier, Amsterdam (658 pp).

Beier, J.A., 1987. Petrographic and geochemical analysis of caliche profiles in a Bahamian Pleistocene dune. Sedimentology 34, 991–998.

Bekele, E.B., Salama, R.B., Commander, D.P., Otto, C.J., Hick, W.P., Watson, G.D., Pollock, D.W., Lambert, P.A., 2003. Estimation of groundwater recharge to the Parmelia Aquifer in the northern Perth Basin 2001–2002. CSIRO Land and Water. Tech. Rep. 10/03 (30 pp).

Bøtter-Jensen, L., Bulur, E., Duller, G.A.T., Murray, A.S., 2000. Advances in luminescence instrument systems. Radiat. Meas. 32, 523–528.

Bottinga, Y., 1969. Calculated fractionation factors for carbon and hydrogen isotope exchange in the system calcite-carbon dioxide-graphite-methane-hydrogen-water vapour. Geochim. Cosmochim. Acta 33, 49–64.

Brooke, B., 2001. The distribution of carbonate eolianite. Earth Sci. Rev. 55, 135–164.

Brooke, B.P., Olley, J.M., Pietsch, T., Playford, P.E., Haines, P.W., Murray-Wallace, C.V., Woodroffe, C.D., 2014. Chronology of Quaternary coastal aeolianite deposition and the drowned shorelines of southwestern Western Australia – a reappraisal. Quat. Sci. Rev. 93, 106–124.

Buhman, D., Dreybrodt, W., 1985. The kinetics of calcite dissolution and precipitation in geologically relevant situations of karst areas. 1. Open systems. Chem. Geol. 48, 189–211.

Bureau of Meteorology, Australian Government, 2016. Climate Statistics for Australian Locations. (URL: http://www.bom.gov.au (February, 2014)).

Burne, R.V., Moore, L.S., 1987. Microbialites: organosedimentary deposits of benthic microbial communities. Palaios 2, 241–254.

Cadman, S.J., Pain, L., Vuclovic, V., 1994. Perth Basin, WA. Australian Petroleum Accumulations Report 10. Canberra, Bureau of Resources Sciences (103 pp).

Carew, J.L., Mylroie, J.E., 1997. Geology of the Bahamas. In: Vacher, H.L., Quinn, T. (Eds.), Geology and Hydrology 54. Elsevier Science, Amsterdam, pp. 91–139.

Cerling, T.E., 1984. The stable isotopic composition of modern soil carbonate and its relationship to climate. Earth Planet. Sci. Lett. 71, 229–240.

Cerling, T.E., Quade, J., 1993. Stable carbon and oxygen isotopes in soil carbonates. In: Swart, P.K., Lohmann, K.C., Mckenzie, J.A., Savin, F. (Eds.), Climate Change in Continental Isotopic Records 78. American Geophysical Union Geophysical Monograph, Washington, D. C., pp. 217–231.

Cox, G., James, J.M., Leggett, K.E.A., Osborne, R.A.L., 1989. Cyanobacterially deposited speleothems: subaerial stromatolites. Geomicrobiol J. 7, 245–252.

Craig, H., 1965. The measurement of oxygen palaeoteomperatures. In: Tongiorgi, E. (Ed.), Stable Isotopes in Oceanographic Studies and Palaeotemperatures. C.N.R. Lab. Geol. Nucleare, Pisa, pp. 161–182.

Cresswell, G.R., 1991. The Leeuwin Current – observations and recent models. J. R. Soc. West. Aust. 74, 1–14.

Davidson, W.A., 1995. Hydrogeology and groundwater resources of the Perth region, Western Australia. Bulletin 142. Western Australia Geological Survey (257 pp).

Deines, P., 1980. The isotopic composition of reduced organic carbon. In: Fritz, P., Fontes, J.C. (Eds.), Handbook of Environmental Isotope Geochemistry 1, The Terrestrial Environment. Elsevier, Amsterdam, pp. 329–406.

Department of Conservation and Land Management, 1998. Nambung National Park Management Plan 1998–2008 (Perth, 64 pp).

Department of Water, 2012. Groundwater Dependent Ecosystem Vulnerability in the Mid West Project (funded by the National Water Commission 2009–2012). Government of Western Australia, Personal Communication.

Desmarchelier, J.M., Goede, A., Ayliffe, L.K., McCulloch, M.T., Moriarty, K., 2000. Stable isotope record and its palaeoenvironmental interpretation for a late Middle Pleistocene speleothem from Victoria Fossil Cave, Naracoorte, South Australia. Quat. Sci. Rev. 19, 763–774.

Dreybrodt, W., 1980. Deposition of calcite from thin films of natural calcareous solutions and the growth of speleothems. Chem. Geol. 29, 89–105.

Dreybrodt, W., Gabrovšek, F., 2002. Climate and early karstification: what can be learned by models? Acta Geol. Pol. 52 (1), 1–11.

Drysdale, R.N., Hellstrom, J.C., Zanchetta, G., Fallick, A.E., Sánchez Goñi, M.F., Couchoud, I., McDonald, J., Maas, R., Lohmann, G., Isola, I., 2009. Evidence for obliquity forcing of glacial termination II. Science 325, 1527–1531.

Dworkin, S.I., Nordt, L., Atchey, S., 2005. Determining terrestrial palaeotemperatures using the oxygen isotopic composition of pedogenic carbonates. Earth Planet. Sci. Lett. 237, 56–68.

Eberhard, S.M., 2004. Ecology and hydrology of a threatened groundwater-dependent ecosystem: the Jewel Cave karst system in Western Australia. (PhD thesis). Murdoch University, School of Environmental Science (321 pp).

Eriksson, E., 1965. Deuterium and oxygen-18 in precipitation and other natural waters. Some theoretical considerations. Tellus 17 (4), 498–512.

Feng, M., Weller, E., Hill, K., 2009. The Leeuwin Current. In: Poloczanska, E.S., Hobday, A.J., Richardson, A.J. (Eds.), A Marine Climate Change Impacts and Adaptation Report Card for Australia 2009. NCCARF Publication 5/9, pp. 1–11.

Flügel, E., 2010. Microfacies of Carbonate Rocks — Analysis, Interpretation and Application. second ed. Springer, Heidelberg, Dordrecht, London, New York (984 pp.).

Ford, D., Williams, P., 2007. Karst Hydrogeology and Geomorphology. John Wiley and Sons, Chichester (562 pp).

Frechen, M., Dermann, B., Boenigk, W., Ronen, A., 2001. Luminescence chronology of aeolianites from the section at Givat Olga – coastal plain of Israel. Quat. Sci. Rev. 20, 805–809.

Friedman, I., O'Neil, J.R., 1977. Compilation of Stable Isotope Fractionation Factor of Geochemical Interest. United States Geological Survey (Professional Paper 440-KK, 12 pp).

Frisia, A., Borsato, A., Fairchild, I.J., McDermott, F., 2000. Calcite fabrics, growth mechanisms, and environments of formations in speleothems from the Italian Alps and southwestern Ireland. J. Sediment. Res. 70, 1183–1196.

Fumanal, M.P., 1995. Pleistocene dune systems in the Valencian Betic cliffs (Spain). INQUA Subcomission on Mediterranean and Black Sea Shorelines Newsletter 17, pp. 32–38.

Galbraith, R.F., Roberts, R.G., Laslett, G.M., Yoshida, H., Olley, J.M., 1999. Optical dating of single and multiple grains of quartz from Jinmium rock shelter, northern Australia: part I, experimental design and statistical models. Archaeometry 41, 339–364.

Gardner, R.A.M., Goudie, A.S., Pye, K., 1983. Aeolianite. Chemical Sediments and Geomorphology: Precipitates and Residua in the Near-surface Environment. Academic Press, pp. 265–300.

Gardner, T.W., Webb, J., Davis, A.G., Cassel, E.J., Pezzia, C., Merritts, D.J., Smith, B., 2006. Late Pleistocene landscape response to climate change: eolian and alluvial fan deposition, Cape Liptrap, southeastern Australia. Quat. Sci. Rev. 25, 1552–1569.

Genty, D., Quinif, Y., 1996. Annually laminated sequences in the internal structure of some Belgian stalagmites—importance for paleoclimatology. J. Sediment. Res. 66, 275–288.

Gingele, F.X., De Deckker, P., Hillenbrand, C.D., 2004. Late Quaternary terrigenous sediments from the Murray Canyons area, offshore South Australia and their implications for sea level change, palaeoclimate and palaeodrainage of the Murray-Darling Basin. Mar. Geol. 212, 183–197.

Gliganic, A.L., Cohen, T.J., May, J.-H., Jansen, J.D., Nanson, G.C., 2014. Late-Holocene climatic variability indicated by three natural archives in arid southern Australia. The Holocene 24 (1), 104–117.

Gouramanis, C., Dodson, J., Wilkins, D., De Deckker, P., Chase, B.M., 2012. Holocene palaeoclimate and sea level fluctuation recorded from the coastal Barker Swamp, Rottnest Island, south-western Western Australia. Quat. Sci. Rev. 54, 40–57.

Gozzard, J.R., 2007. Geology and Landforms of the Perth Region. Western Australia Geological Survey (126 pp).

Green, H., Pickering, R., 2014. The influence of the Austral Westerlies recorded in new Late Pleistocene stalagmites from South Africa. Scientific Programme and Abstracts from the Climate Change: The Karst Record, 7th International Conference in Melbourne, Australia, pp. 87–88.

Grimes, K.G., 2006. Syngenetic karst in Australia: a review. Helictite 39 (2), 27–38.

Grimes, K.G., 2009. Solution pipes and pinnacles in syngenetic karst. In: Gines, A., Knez, M., Slabe, T., Dreybrodt, W. (Eds.), Karst Rock Features, Karren Sculpturing. Založba ZRC SAZU, Ljubljana – Postojna, pp. 513–523.

Guérin, G., Mercier, N., Adamiec, G., 2011. Dose rate conversion factors: update. Ancient TL 29, 5–8.
Harrison, S.P., 1993. Late Quaternary lake-level changes and climates of Australia. Quat. Sci. Rev. 12, 211–231.
Harle, K.J., 1997. Late Quaternary vegetation and climate change in southeastern Australia: palynological evidence from marine core E55-6. Palaeogeogr. Palaeoclimatol. Palaeoecol. 131, 465–483.
Hattersley, P.W., 1983. The distribution of C3 and C4 grasses in Australia in relation to climate. Oecologia (Berlin) 57, 113–128.
Hauser, S., Dongarrà, G., Favara, R., Longinelli, A., 1980. Composizione isotopica delle piogge in Sicilia. Riferimenti di base per studi idrogeologici e relazioni con altre aree Mediterranee. Societa Italiana di Mineralogia e petrologia 36 (2), 671–680.
Hays, P.D., Grossman, E.L., 1991. Oxygen isotopes in meteoric calcite cements as indicators of continental palaeoclimate. Geology 19, 441–444.
Hearty, P.J., 2003. Stratigraphy and timing of eolianite deposition on Rottnest Island, Western Australia. Quat. Res. 60, 211–222.
Hearty, P.J., Kindler, P., 1997. The stratigraphy and surficial geology of New Providence and surrounding islands, Bahamas. J. Coast. Res. 13, 798–812.
Hearty, P.J., O'Leary, M.J., 2008. Carbonate aeolianites, quartz sands, and Quaternary sea-level cycles, Western Australia: a chronostratigraphic approach. Quat. Geochronol. 3, 26–55.
Hearty, P.J., Olson, S.L., 2011. Preservation of trace fossils and molds of terrestrial biota by intense storms in mid-last interglacial (MIS 5c) dunes on Bermuda, with a model for development of hydrological conduits. Palaios 26, 394–405.
Hearty, P.J., Vacher, H.L., 1994. Quaternary stratigraphy of Bermuda: a high-resolution pre-Sangamonian rock record. Quat. Sci. Rev. 13, 685–697.
Hellstrom, J., 2003. Rapid and accurate U/Th dating using parallel ion-counting multi-collector ICP-MS. J. Anal. At. Spectrom. 18, 1346–1351.
Hellstrom, J., 2006. U–Th dating of speleothems with high initial $^{230}$Th using stratigraphical constraint. Quat. Geochronol. 1, 289–295.
James, N.P., Bone, Y., 2015. Pleistocene aeolianites at Cape Spencer, South Australia; record of a vanished inner neritic cool-water carbonate factory. Sedimentology 62 (7), 2038–2059.
Jenkin, J.J., 1984. Evolution of the Australian coast and continental margin. In: Thom, B.G. (Ed.), Coastal Geomorphology in Australia. Academic Press (0349 pp).
Jennings, J.N., 1968. Syngenetic Karst in Australia: Contributions to the Study of Karst. The Australian National University, Research School of Pacific Studies, Department of Geography Publication G/5, pp. 41–110.
Jennings, J.N., Mabbutt, J.A., 1977. Physiographic outlines and regions. In: Jeans, D.M. (Ed.), Australia, a Geography. University of Sydney Press, Sydney, pp. 38–52.
Jiamao, H., Keppens, E., Tungsheng, L., Paepe, R., Wenying, J., 1997. Stable isotope composition of the carbonate concretion in loess and climate change. Quat. Int. 37, 37–43.
Johnstone, D., Playford, P.E., 1955. Geology of the Shark Bay-Murchison River Area. West Australian Petroleum Pty Ltd Rept, Carnarvon Basin (unpublished).
Jouzel, J., Masson-Delmotte, V., Cattani, O., Dreyfus, G., Falourd, S., Hoffmann, G., Minster, B., Nouet, J., Barnola, J.M., Chappellaz, J., Fischer, H., Gallet, J.C., Johnsen, S., Leuenberger, M., Loulergue, L., Luethi, D., Oerter, H., Parrenin, F., Raisbeck, G., Raynaud, D., Schilt, A., Schwander, J., Selmo, E., Souchez, R., Spahni, R., Stauffer, B., Steffensen, J.P., Stenni, B., Stocker, T.F., Tison, J.L., Werner, M., Wolff, E.W., 2007. Orbital and millennial Antarctic climate variability over the past 800,000 years. Science 317, 793–797.
Kaye, C.A., 1959. Geology of the San Juan Metropolitan Area Puerto Rico. Geological Survey Professional Paper 317-A (48 pp).
Kendrick, G.W., 1977. Middle Holocene marine molluscs from near Guildford, Western Australia and evidence for climatic change. J. R. Soc. West. Aust. 59, 97–104.
Kendrick, G.W., Wyrwoll, K.H., Szabo, B.J., 1991. Pliocene-Pleistocene coastal events and history along the western margin of Australia. Quat. Sci. Rev. 10, 419–439.
Kershaw, A.P., Nanson, G.C., 1993. The last full glacial cycle in the Australian region. Glob. Planet. Chang. 7, 1–9.
Kim, S.T., Mucci, A., Taylor, B., 2007. Phosphoric acid fractionation factors for calcite and aragonite between 25 and 75 °C: revisited. Chem. Geol. 246, 135–146.
Kindler, P., Hearty, P.J., 1996. Carbonate petrography as an indicator of climate and sea-level changes: new data from Bahamian Quaternary units. Sedimentology 43, 381–399.
Klappa, C.F., 1980. Rizoliths in terrestrial carbonates: classification, recognition, genesis and significance. Sedimentology 27 (6), 613–629.
Küçükuysal, C., Türkmenoğlu, A.G., Kapur, S., 2012. Multiproxy evidence of Mid-Pleistocene dry climates observed in calcretes in Central Turkey. Turk. J. Earth Sci. 21, 1–17.
Lemieux-Dudon, B., Blayo, E., Petit, J.R., Waelbroeck, C., Svensson, A., Ritz, C., Barnola, J.M., Narcisi, B.M., Parrenin, F., 2010. Consistent dating for Antarctic and Greenland ice cores. Quat. Sci. Rev. 29 (1–2), 8–20.
Liotta, M., Grassa, F., D'Alessandro, W., Favara, R., Gagliano Candela, E., Pisciotta, A., Scaletta, C., 2013. Isotopic composition of precipitation and groundwater in Sicily, Italy. Appl. Geochem. 34, 199–206.
Lipar, M., 2009. Pinnacle syngenetic karst in Nambung National Park, Western Australia. Acta Carsologica 38 (1), 41–50.
Lipar, M., Webb, J.A., 2014. Middle – Late Pleistocene and Holocene chronostratigraphy and depositional history of the Tamala Limestone, Cooloongup and Safety Bay sands, Nambung National Park, southwestern Western Australia. Aust. J. Earth Sci. 61, 1023–1039.
Lipar, M., Webb, J.A., 2015. The formation of the pinnacle karst in Pleistocene aeolian calcarenites (Tamala limestone) in southwestern Australia. Earth Sci. Rev. 140, 182–202.
Lipar, M., Webb, J.A., White, S.Q., Grimes, K.G., 2015. The genesis of solution pipes: evidence from the Middle-Late Pleistocene Bridgewater Formation calcarenites, southeastern Australia. Geomorphology 246, 90–103.
Lomax, J., Hilgers, A., Radtke, U., 2011. Palaeoenvironmental change recorded in the palaeodunefields of the western Murray Basin, South Australia – new data from single OSL-dating. Quat. Sci. Rev. 30, 723–736.
Lowry, D.C., 1973. Origin of the Pinnacles, Nambung, WA. 62. ASF Newsletter, pp. 7–8.
Lundberg, J., McFarlane, D.A., 2011. Subaerial freshwater phosphatic stromatolites in Deer Cave, Sarawak – a unique geobiological cave formation. Geomorphology 128, 57–72.
Luntz, S., 2004. Leeuwin Current the world's longest. Australas. Sci. 25 (5), 8.
Markey, B.G., Bøtter-Jensen, L., Duller, G.A.T., 1997. A new flexible system for measuring thermally and optically stimulated luminescence. Radiat. Meas. 27, 83–89.
Martinez, J.I., De Deckker, P., Barrows, T., 1999. Palaeoceanography of the last glacial maximum in the eastern Indian Ocean: planktonic foraminifera evidence. Palaeogeogr. Palaeoclimatol. Palaeoecol. 147, 73–99.
McNamara, K., 2009. Pinnacles. Perth, Western Australian Museum (62 pp).
Mejdahl, V., 1979. Thermoluminescence dating: beta-dose attenuation in quartz grains. Archaeometry 21, 61–72.
Milnes, A.R., Kimber, R.W., Phillips, S.E., 1987. Studies in calcareous aeolian landscapes of Southern Australia. In: Liu, T. (Ed.), Aspects of Loess Research. China Ocean Press, pp. 130–139.
Molina-Cruz, A., 1977. The relation of the southern trade winds to upwelling processes during the last 75,000 years. Quat. Res. 8, 324–338.
Mory, A.J., 1995. Geology of the Wedge island 1:100.000 sheet. Geological Survey of Western Australia, Perth (19 pp. and geologic map).
Muhs, D.R., Whelan, J.F., Kennedy, G.L., Rockwell, T.K., 1993. Late Quaternary sea level history of the pacific coast of North America: a detailed record of the Last Glacial/Interglacial cycle. In: Kelmelis, J.A., Snow, M. (Eds.), US Geological Survey Global Change Research Forum. US Geological Survey, Herndon, VA, pp. 101–102.
Murray, A.S., Roberts, R.G., 1998. Measurement of the equivalent dose in quartz using a regenerative-dose single-aliquot protocol. Radiat. Meas. 29, 503–515.
Murray, A.S., Wintle, A.G., 2000. Luminescence dating of quartz using an improved single-aliquot regenerative-dose protocol. Radiat. Meas. 32, 57–73.
Murray-Wallace, C.V., 2002. Pleistocene coastal stratigraphy, sea-level highstands and neotectonism of the southern Australian passive continental margin—a review. J. Quat. Sci. 17, 469–489.
Murray-Wallace, C.V., Belperio, A.P., Cann, J.H., 1998. Quaternary neotectonism and intraplate volcanism: the Coorong to Mount Gambier Coastal Plain, Southeastern Australia: a review. In: Vita Finzi, C., Stewart, C. (Eds.), Coastal Tectonics. Geological Society, London, pp. 255–267.
Murray-Wallace, C.V., Beu, A.G., Kendrick, G.W., Brown, L.J., Belperio, A.P., Sherwood, J.E., 2000. Palaeoclimatic implications of the occurrence of the arcoid bivalve Anadara trapezia (Deshayes) in the Quaternary of Australasia. Quat. Sci. Rev. 19, 559–590.
Murray-Wallace, C.V., Bourman, R.P., Prescott, J.R., Williams, F., Price, D.M., Belperio, A.P., 2010. Aminostratigraphy and thermoluminescence dating of coastal aeolianites and the later Quaternary history of a failed delta: the River Murray mouth region, South Australia. Quat. Geochronol. 5, 28–49.
Murray-Wallace, C.V., Brooke, B.P., Cann, J.H., Belperio, A.P., Bourman, R.P., 2001. Whole-rock aminostratigraphy of the Coorong Coastal Plain, South Australia: towards a 1 million year record of sea-level highstands. J. Geol. Soc. Lond. 158, 111–124.
Mylroie, J.E., 2008. Late Quaternary sea-level position: evidence from Bahamian carbonate deposition and dissolution cycles. Quat. Int. 183, 61–75.
Nanson, G.C., Cohen, T.J., Doyle, C.J., Price, D.M., 2003. Alluvial evidence of major Late-quaternary climate and flow-regime changes on the coastal rivers of New South Wales, Australia. In: Gregory, K.J., Bentilo, G. (Eds.), Palaeohydrology – Understanding Global Change. John Wiley, pp. 233–258.
Nanson, G.C., Price, D.M., Short, S.A., 1992. Wetting and drying of Australia over the past 300 ka. Geology 20, 791–794.
Pain, C., Gregory, L., Wilson, P., McKenzie, N., 2011. The Physiographic Regions of Australia: Explanatory Notes. Australian Collaborative Land Evaluation Program and National Committee on Soil and Terrain (30 pp).
Parkin, D.W., 1974. Trade-winds during the glacial cycles. Proc. R. Soc. Lond. A Math. Phys. Sci. 337 (1608), 73–100.
Passmore, J.R., 1970. Shallow coastal aquifers in the Rockingham District, Western Australia. 18. Water Research Foundation Australia Bulletin (83 pp).
Pickett, E.J., Harrison, S.P., Hope, G., Harle, K., Dodson, J.R., Kershaw, A.P., Prentice, I.C., Backhouse, J., Colhoun, E.A., D'Costa, D., Flenley, J., Grindrod, J., Haberle, S., Hassel, C., Kenyon, C., Macphail, M., Martin, H., Martin, A.H., McKenzie, M., Newsome, J.C., Penny, D., Powell, J., Raine, J.I., Southern, W., Stevenson, J., Sutra, J.-P., Thomas, I., van der Kaars, S., Ward, J., 2004. Pollen-based reconstructions of biome distributions for Australia, Southeast Asia and the Pacific (SEAPAC region) at 0, 6000 and 8,000 $^{14}$C yr BP. J. Biogeogr. 31, 1381–1444.
Playford, P.E., 1990. Geology of the Shark Bay area, Western Australia. In: Berry, P.F., Bradshaw, S.D., Wilson, B.R. (Eds.), Research in Shark Bay. Report of the France-Australe Bicentenary Expedition Committee. Western Australian Museum, Perth, pp. 13–31.
Playford, P.E., 1997. Geology and hydrogeology of Rottnest Island, Western Australia. In: Vacher, H.L., Quinn, T. (Eds.), Geology and Hydrogeology of Carbonate IslandsDevelopments in Sedimentology 54. Elsevier Science, pp. 783–810.
Playford, P.E., Cockbain, A.E., Berry, P.F., Roberts, A.P., Haines, P.W., Brooke, B.P., 2013. The Geology of Shark Bay. 146. Geological Survey of Western Australia Bulletin (281 pp).
Playford, P.E., Cockbain, A.E., Low, G.H., 1976. Geology of the Perth Basin Western Australia. Geological Survey of Western Australia Bulletin. 124 (311 pp).
Playford, P.E., Low, G.H., 1971. Definitions of some new and revised rock units in the Perth Basin. Western Australia Geological Survey, Annual Report. 1971, pp. 44–46.
Porat, N., Botha, G., 2008. The luminescence chronology of dune development on the Maputaland coastal plain, southeast Africa. Quat. Sci. Rev. 27, 1024–1046.
Prescott, J.R., Hutton, J.T., 1994. Cosmic ray contributions to dose rates for luminescence and ESR dating: large depths and long-term time variations. Radiat. Meas. 23, 497–500.

Price, D.M., Brooke, B.P., Woodroffe, C.D., 2001. Thermoluminescence dating of aeolianites from Lord Howe Island and South-West Western Australian. Quat. Sci. Rev. 20, 841–846.
Quade, J., Cerling, T.E., Bowman, J.R., 1989. Systematic variations in the carbon and oxygen isotopic composition of pedogenic carbonates along elevation transects in the southern Great Basin, United States. Geol. Soc. Am. Bull. 101, 46–475.
Reason, C.J.C., Gamble, D., Pearce, A.F., 1999. The Leeuwin Current in the Parallel Ocean Climate Model and applications to regional meteorology and fisheries. Meteorol. Appl. 6 (3), 211–225.
Reeckmann, S.A., Gill, E.D., 1981. Rates of vadose diagenesis in Quaternary dune and shallow marine calcarenites, Warrnambool, Victoria, Australia. Sediment. Geol. 30, 157–172.
Rognon, P., Williams, M.A.J., 1977. Late quaternary climatic changes in Australia and North Africa: a preliminary interpretation. Palaeogeogr. Palaeoclimatol. Palaeoecol. 21 (4), 285–327.
Rojas, M., Moreno, P., Kageyama, M., Crucifix, M., Hewitt, C., Abe-Ouchi, A., Ohgaito, R., Brady, E.C., Hope, P., 2009. The Southern Westerlies during the last glacial maximum in PMIP2 simulations. Clim. Dyn. 32 (4), 525–548.
Rozanski, K., Araguás-Araguás, L., Gonfiantini, R., 1992. Relation between long-term trends of oxygen-18 isotope composition of precipitation and climate. Nature 258, 981–985.
Scholle, P.A., 1978. A color illustrated guide to carbonate rock constituents, textures, cements, and porosities. The American Association of Petroleum Geologists, Memoir 27, Tulsa (241 pp).
Semeniuk, V., 1983. The Quaternary stratigraphy and geological history of the Australind-Leschenault Inlet area. J. R. Soc. West. Aust. 66 (3), 71–83.
Semeniuk, V., 1985. The age structure of a Holocene barrier dune system and its implication for sealevel history reconstructions in southwestern Australia. Mar. Geol. 67, 197–212.
Semeniuk, V., 1986. Holocene climate history of coastal southwestern Australia using calcrete as an indicator. Palaeogeogr. Palaeoclimatol. Palaeoecol. 53, 289–308.
Semeniuk, V., Cresswell, I.D., Wurm, P.A.S., 1989. The Quindalup Dunes: the regional system, physical framework and vegetation habitats. J. R. Soc. West. Aust. 71 (2and3), 23–47.
Shulmeister, J., Goodwin, I., Renwick, J., Harle, K., Armand, L., McGlone, M.S., Cook, E., Dodson, J., Hesse, P.P., Mayewski, P., Curran, M., 2004. The Southern Hemisphere westerlies in the Australasian sector over the last glacial cycle: a synthesis. Quat. Int. 118–119, 23–53.
Sijp, W.P., England, M.H., 2008. The effect of a northward shift in the southern hemisphere westerlies on the global ocean. Prog. Oceanogr. 79, 1–19.
Sikes, N.E., Ashley, G.M., 2007. Stable isotopes of pedogenic carbonates as indicators of paleoecology in the Plio-Pleistocene (upper bed I), western margin of the Olduvai Basin, Tanzania. J. Hum. Evol. 53, 574–594.
Smith, D.I., Atkinson, T.C., 1976. Process, landforms and climate in limestone regions. In: Derbyshire, E. (Ed.), Geomorphology and Climate. John Wiley, London, pp. 367–409.
Spooner, M.I., De Deckker, P., Barrows, T.T., Fifield, L.K., 2011. The behaviour of the Leeuwin Current offshore NW Australia during the last five glacial-interglacial cycles. Glob. Planet. Chang. 75, 119–132.
Stuut, J.-B.W., Temmesfeld, F., De Deckker, P., 2014. A 550 ka record of aeolian activity near North West Cape, Australia: inferences from grain-size distributions and bulk chemistry of SE Indian Ocean deep-sea sediments. Quat. Sci. Rev. 83, 83–94.
Tabor, N.J., Montanez, I.P., Southard, R.J., 2002. Palaeoenvironmental reconstruction from chemical and isotopic compositions of Permo-Pennsylvanian pedogenic minerals. Geochim. Cosmochim. Acta 66, 3093–3107.
Tabor, N.J., Montanez, I.P., 2005. Oxygen and hydrogen isotope composition of Permian pedogenic phyllosilicates: development of modern surface domain arrays and implications for palaeotemperatures reconstructions. Palaeogeogr. Palaeoclimatol. Palaeoecol. 223, 127–146.
Tapsell, P., Newsome, D., Bastian, L., 2003. Origin of yellow sand from Tamala Limestone on the Swan Coastal Plain, Western Australia. Aust. J. Earth Sci. 50, 331–342.
Teichert, C., 1947. Stratigraphy of Western Australia. J. Proc. R. Soc. NSW 80, 81–142.
Teichert, C., 1950. Late Quaternary changes of sea-level at Rottnest Island, Western Australia. Proc. Roy. Soc. Victoria 59, 63–79.
Toggweiler, J.R., Russell, J.L., Carson, S.R., 2005. Midlatitude westerlies, atmospheric $CO_2$, and climate change during the ice ages. Paleoceanography 21, 1–15.
Tremaine, D.M., Froelich, P.N., Wang, Y., 2011. Speleothem calcite farmed in situ: Modern calibration of $\delta^{18}O$ and $\delta^{13}C$ paleoclimate proxies in a continuously-monitored natural cave system. Geochim. Cosmochim. Acta 75, 4929–4950.
Turner, J.V., Thorpe, P.M., 2002. Palaeotemperature conditions for the southwest of Western Australia from the stable isotopic composition of deep, confined groundwater within the Perth Basin. Report. Proceedings of the Study of Environmental Change Using Isotope Techniques. International Atomic Energy Agency, pp. 504–508.
Turney, C.S.M., Haberle, S., Fink, D., Kershaw, A.P., Barbetti, M., Barrows, T.T., Black, M., Cohen, T.J., Corrége, T., Hesse, P.P., Hua, Q., Johnston, R., Morgan, V., Moss, P., Nanson, G., Van Ommen, T., Rule, S., Williams, N.J., Zhao, J.X., D'Costa, D., Feng, Y.X., Gagan, M., Mooney, S., Xia, Q., 2006. Integration of ice-core, marine and terrestrial records for the Australian Last Glacial Maximum and Termination: a contribution from the OZ INTIMATE group. J. Quat. Sci. 21 (7), 751–761.
Waelbroeck, C., Labeyrie, L., Michel, E., Duplessy, J.C., McManus, J., Lambeck, K., Balbon, E., Labracherie, M., 2002. Sea-level and deep water temperature changes derived from benthic foraminifera isotopic records. Quat. Sci. Rev. 21, 295–305.
Wang, Y., Zheng, S.H., 1989. Paleosol nodules as Pleistocene paleoclimatic indicators, Luochuan, P. R. China. Palaeogeogr. Palaeoclimatol. Palaeoecol. 76, 39–44.
Ward, W.C., 1973. Influence of climate on the early diagenesis of carbonate eolianites. Geology 1 (4), 171–174.
White, W.B., 1988. Geomorphology and Hydrology of Karst Terrains. Oxford University Press, New York (464 pp).
Williams, A.H., Walkden, G.M., 2002. Late Quaternary highstand deposits of the southern Arabian Gulf: a record of sea-level and climate change. Geol. Soc. Lond., Spec. Publ. 195, 371–386.
Williams, M., Cook, E., van der Kaars, S., Barrows, T., Shulmeister, J., Kershaw, P., 2009. Glacial and deglacial climatic patterns in Australia and surrounding regions from 35000 to 10000 years ago reconstructed from terrestrial and near-shore proxy data. Quat. Sci. Rev. 28, 2398–2419.
Wright, V.P., 1988. Paleokarsts and paleosols as indicators of paleoclimate and porosity evolution: a case study from the Carboniferous of South Wales. In: James, N.P., Choquette, P.W. (Eds.), Paleokarst. Springer-Verlag, New York, Berlin, Heidelberg, London, Paris, Tokyo, pp. 329–341.
Wright, V.P., 1989. Terrestrial stromatolites and laminar calcretes: a review. Sediment. Geol. 65, 1–13.
Wyrwoll, K.H., 1979. Late Quaternary climates of Western Australia: evidence and mechanisms. J. R. Soc. West. Aust. 62, 129–142.
Wyrwoll, K.H., 1993. An outline of Late Cenozoic palaeoclimatic events in the Cape Range region. In: Humphreys, W.F. (Ed.), The Biogeography of Cape Range, Western Australia. Western Australian Museum, Perth, pp. 39–50.
Yassini, I., Kendrick, G.W., 1988. Middle Holocene ostracodes, foraminifers and environments of beds at Point Waylen, Swan River Estuary, southwestern Australia. Alcheringa 12, 107–121.
Zanchetta, G., Di Vito, M., Fallick, A.E., Sulpizio, R., 2000. Stable isotopes of pedogenic carbonates from the Somma-Vesuvius area, southern Italy, over the past 18 kyr: palaeoclimatic implications. J. Quat. Sci. 15 (8), 813–824.
Zhao, J.-X., Yu, K.-F., Feng, Y.-X., 2009. High-precision $^{238}U$–$^{234}U$–$^{230}Th$ disequilibrium dating of the recent past: a review. Quat. Geochronol. 4, 423–433.
Zheng, H., Powell, C.M., Zhao, H., 2002. Eolian and lacustrine evidence of late Quaternary palaeoenvironmental changes in southwestern Australia. Glob. Planet. Chang. 35, 75–92.